Grant Agreement No: 101096307

Full Title: THz Industrial Mesh Networks in Smart Sensing and Propagation Environments

Start date: 01/01/2023

End date: 31/03/2026

Duration: 39 Months

Deliverable D6.3

Full integration of the 300 GHz PoC

Document Type	Deliverable
Title	D6.3 – Full integration of the 300 GHz PoC
Contractual due date	31/01/2026
Actual submission date	06/02/2026
Nature	Report
Dissemination Level	Public
Lead Beneficiary	CNRS
Responsible Author	G. Ducournau (CNRS)
Contributions from	F. Dutin (CNRS), S. Kroos (TUBS)

Revision history

Version	Issue Date	Changes	Contributor(s)
v0.1	15/01/2026	Parts related to PoC1	F. Dutin (CNRS)
v0.2	20/01/2026	Parts related to PoC2	S. Kroos (TUBS)
V1.0	05/02/2026	Assembly, writing, editing PoC1 and review	G. Ducournau (CNRS)
V1.1	06/02/2026	Typos & editing	G. Ducournau (CNRS)
N/A	11/02/2026	Review	L. Sanguinetti (CNIT) S. Chartier (IAF)
V2.0	12/02/2026	Corrections	G. Ducournau (CNRS)
V2.1	16/02/2026	Final version	L.Sanguinetti (CNIT), T. Kurner (TUBS)

Table of Contents

List of Abbreviations

AoA Angle of Arrival
AoD Angle of Departure
B2B Back-to-back (direct connection with waveguides)
BS Base Station
CINR Carrier to Interference and Noise Ratio (dB)
FDD Frequency Division Duplex
FWG Flexible Waveguide
IDU TIMES Indoor Units (Tx and Rx converters)
IF Intermediate Frequency
LNA Low Noise Amplifier
LO Local Oscillator
LWA Leaky-Wave Antenna
MPA Medium Power Amplifier
MS Mobile Station
NLoS Non-Line of Sight
OTA Over The Air
PHY Physical Layer
PLL Phase Locked Loop
PoC Proof of Concept
RF Radio Frequency
RIS Reconfigurable Intelligent Surface
RSSI Received Signal Strength Indicator (dBm)
TDD Time Division Duplex
THz Terahertz
VA Variable Attenuator
VNA Vector Network Analyzer

Executive Summary

This document reports on the integration of the RF Front-ends, antennas and RIS towards the preparation of the TIMES Proof of Concepts (PoCs) demos. These PoCs are based on TIMES developed hardware, some of these being used for PoC1 only or PoC2 only, whereas some being common for both PoCs.

1. Introduction

1.1 Scope

This deliverable provides a summary of the integration phase for both PoC1 and PoC2.

1.2 Audience

This report is intended for internal use by the TIMES Consortium and public dissemination.

1.3 Structure

The rest of the document is structured as follows:

- Section 2 presents the PoC1 and related hardware.
- Section 3 presents the PoC2 and related hardware.
- Section 4 presents the conclusions related to PoC1 and PoC2, at this time as the 2 PoCs are still running for preparation of the final demos.

2 PoC-1 : Point-to-Point THz Link over RIS

2.1 Introduction and Goals

The industrial scenario has been updated from the initial plans described in the D2.3. “Definition of the scenarios and KPI for hardware demonstration and PoC” [1], while keeping the same overall concept.

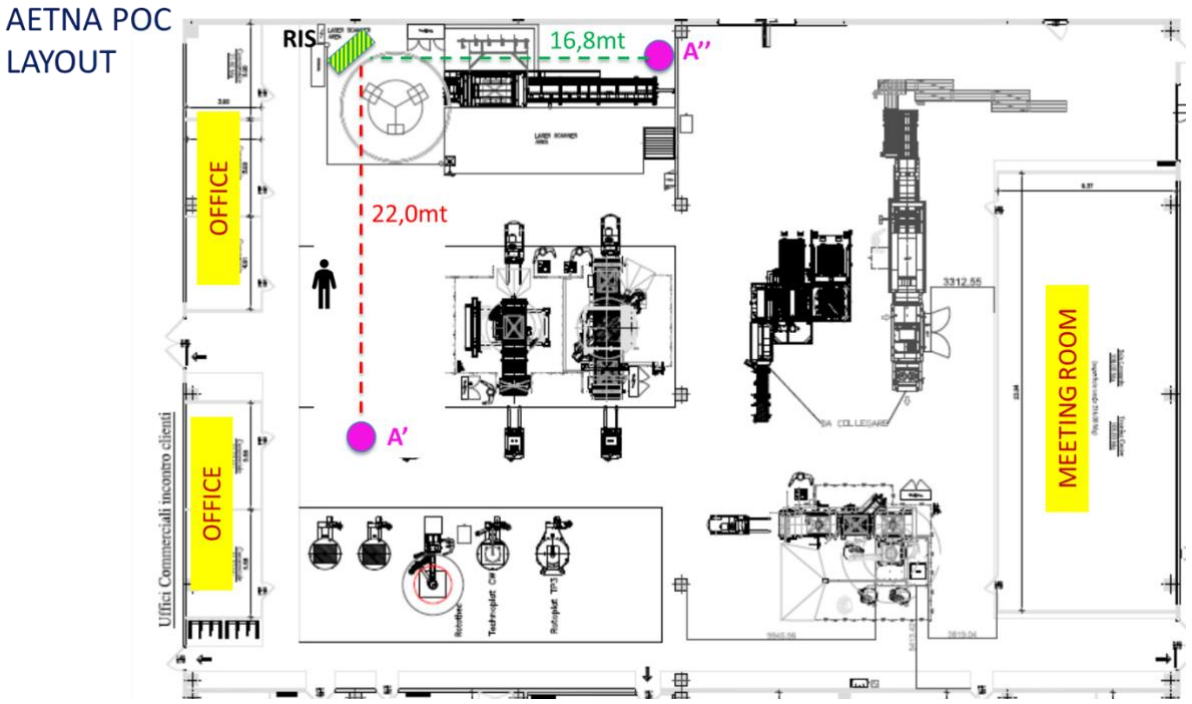

Fig.1. Scenario of the PoC1: A THz NLoS link is established between A’ and A”, these two points being located in an industrial environment at AETNA / Techlab.

The NLoS link is achieved using the RIS approach, where the reflection of the THz signal on the RIS is a non-specular case. Details are given afterwards.

2.2 System Overview

This section gives a recap of the system overview and hardware types that are the essential building blocks for the experimental demonstrations. This includes several types of hardware, active/passive, static/dynamic.

Among the different building blocks of any THz link, that is the physical PHY layer associated to the PoC, the following hardware is to be part of the link:

- Antenna, used as an interface from waveguide-based to free-space. Two types of antennas are considered here: i) fixed/high gain and ii) beam-steerable antenna.

The two types of antenna are characterized and tested as reported in the TIMES deliverable D3.4 “Characterisation of IRS, high directivity antennas and beam steering antennas at sub-THz frequencies”

- Transmit and receive (T/R) integrated circuits (integrated in modules), that make the link with MODEMS. These units enable to up or down-convert the signals from the MODEMS to the 300 GHz band, and include the required local oscillators (LO) as well as the amplification stages at Tx side (MPA) and Rx (LNA).

The performances of these THz sub-systems are described in the TIMES deliverable D6.2 “Integration and validation of MODEM+RF Front ends”

- MODEMS, that enable to connect the network interfaces to the IF front-end interfaces of the T/R modules, before up/down conversion to the 300 GHz band.

MODEMs and associated performances are described in the TIMES deliverable D6.2 “Integration and validation of MODEM+RF Front ends”

- IRS (Intelligent Reflective Surfaces), that are inserted within the THz channel (in the THz path), enabling NLoS connections using THz frequencies (here the 300 GHz band).

The performances of the IRS are described in the deliverable D5.4 “Development and validation of IRS-based THz links”

Based on these components, the overview of the end-to-end assembly that is targeting to connect any machine using the 300 GHz radio spectrum is given hereafter by the Figure 2:

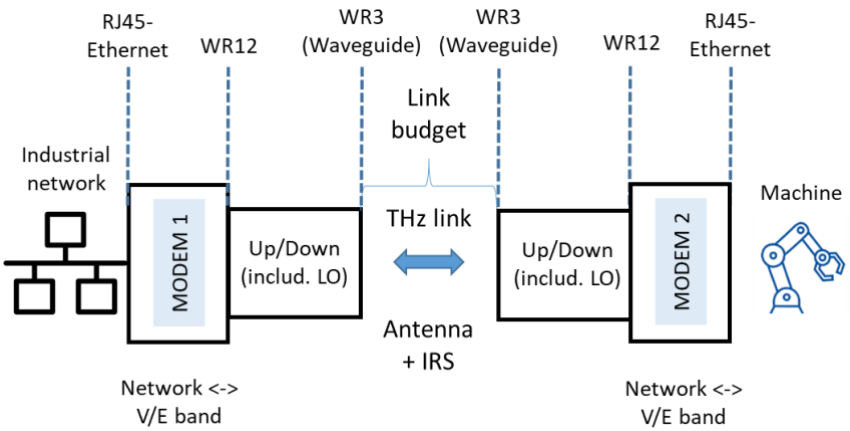

Fig. 2. End-to-end connection of a machine using ethernet/THz/ethernet bridge. The modem architecture can time domain (TDD) based (PoC2), and uses frequency domain duplex (FDD) in PoC1.

In this approach, two types of MODEMS are used for TIMES PoCs. For the PoC1, the MODEM type is a FDD (Frequency Division Duplex), whereas in the PoC2 the MODEM is TDD.

2.2.1 Radio System and Link Budget

2.2.1.1 Block diagram

Figure 3 shows the block diagrams of the transmitter and receiver with high-gain antennas and RIS. The given frequency values are those already determined and presented in deliverable D6.2 and are also specified in Figures 3 and 4.

We will only describe the transmitter section since the receiver section is identical. The FDD modem generates an IF signal in the E-band between 70 and 90 GHz. It has two inputs: one 1 Gbps Ethernet input for PoE power and one 10 Gbps Ethernet input connected to a PC (PC 1) on which iperf is installed. This software allows testing the data transfer speed to the other FDD modem in the receiver section. The IF signal is up-converted using a PLL-generated local oscillator (LO), producing an RF signal in the WR3.4 band between 275 and 320 GHz.

Different attenuators are used in order to prevent any saturation of the IDUs. It is important to note that a variable attenuator (VA) is present to reduce the signal power reaching the IDU. On the receiver side, the process is reversed. The RF signal is received and then down-converted via the PLL to obtain an E-band signal.

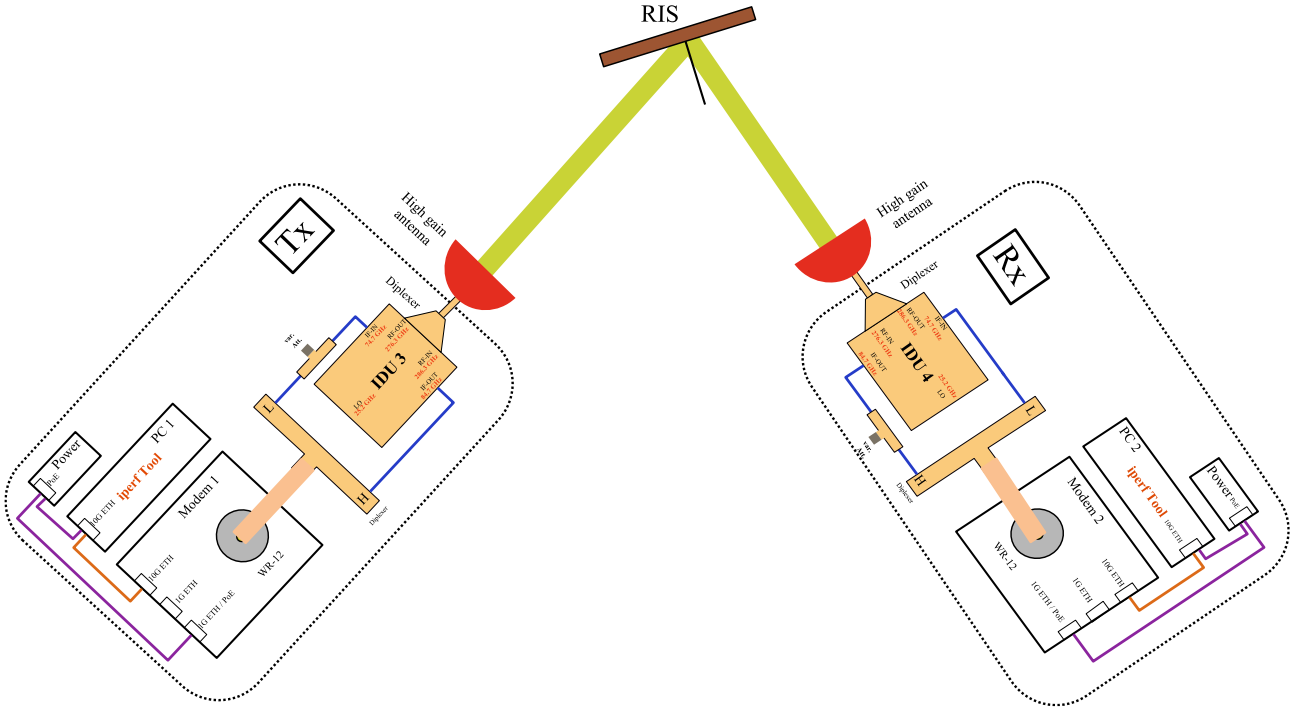

Figure 3: Block diagram of the PoC demonstrator. All devices and frequencies are shown as well as high-gain antennas and RIS.

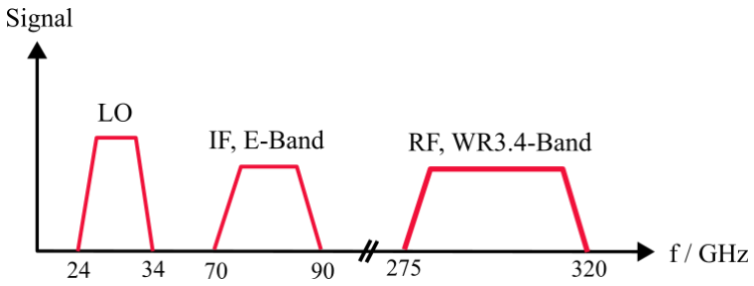

Figure 4: Frequency ranges of LO, IF and RF. For OTA tests, free space propagation is only the WR3.4 band.

2.2.1.2 Link budget

For the PoC1 demonstrator, the link budget that was estimated in the D2.3 [1] has been updated according to the updated plan for the PoC. It is written in the form:

$$L_{\mathrm{Tx-Rx}} = G_{\mathrm{Tx-ant}} - L_{\mathrm{FSPL}}^{\mathrm{Tx-Rx}} - L_{\mathrm{RIS}} + G_{\mathrm{Rx-ant}}$$

with $G_{\mathrm{Tx-ant}} = G_{\mathrm{Rx-ant}}$ being the gain of the high-gain antennas, $L_{\mathrm{FSPL}}^{\mathrm{Tx-Rx}}$ the total free space pathloss along the 39 m path and L_{RIS} the RIS losses. These quantities are calculated at the highest and lowest frequencies of the modems after up-conversion, i.e., 276.3 and 286.3 GHz.

Total free space pathloss is written in the form

$$L_{\mathrm{FSPL}}^{\mathrm{Tx-Rx}}(f) = 20\log_{10}(d_{\mathrm{km}}) + 20\log_{10}(f) + 92.45$$

with d in km and f in GHz. By taking the total distance Tx -> RIS -> Rx = 39 m, we obtain

$$L_{\mathrm{FSPL}}^{\mathrm{Tx-Rx}}(f = 276.3\ \mathrm{GHz}) \approx 113\ \mathrm{dB}$$

$$L_{\mathrm{FSPL}}^{\mathrm{Tx-Rx}}(f = 286.3\ \mathrm{GHz}) \approx 113.3\ \mathrm{dB}$$

According to information in deliverable D5.3 [2], the gain of high-gain antennas is

$$G_{\mathrm{Tx-ant}}(f = 276.3\ \mathrm{GHz}) \approx 53.3\ \mathrm{dBi}$$

$$G_{\mathrm{Tx-ant}}(f = 286.3\ \mathrm{GHz}) \approx 53.4\ \mathrm{dBi}$$

Finally, according to the information in deliverable D5.4 [3], the RIS losses are

$$L_{\mathrm{RIS}}(f = 276.3\ \mathrm{GHz}) \approx 6.8\ \mathrm{dB}$$

$$L_{\mathrm{RIS}}(f = 286.3\ \mathrm{GHz}) \approx 6.3\ \mathrm{dB}$$

Thus, we finally find

$$L_{\mathrm{Tx-Rx}}(f = 276.3\ \mathrm{GHz}) = 13.2\mathrm{dB}$$

$$L_{\mathrm{Tx-Rx}}(f = 286.3\ \mathrm{GHz}) = 12.8\ \mathrm{dB}$$

These values will be compared to the system's possible margin detailed at the end of the section 2, for each modulation that were determined with a direct (back-to-back) connection using calibrated waveguides.

2.2.2 Installation, Positioning and Wiring for AETNA PoC

The overall plan has been given in Figure 1, while the Figure 5 shows details about the definition of the connections, that are fixed at this time. While the detailed descriptions will be part of the D6.4, here we show some of the key features to assess the details of the final PoC.

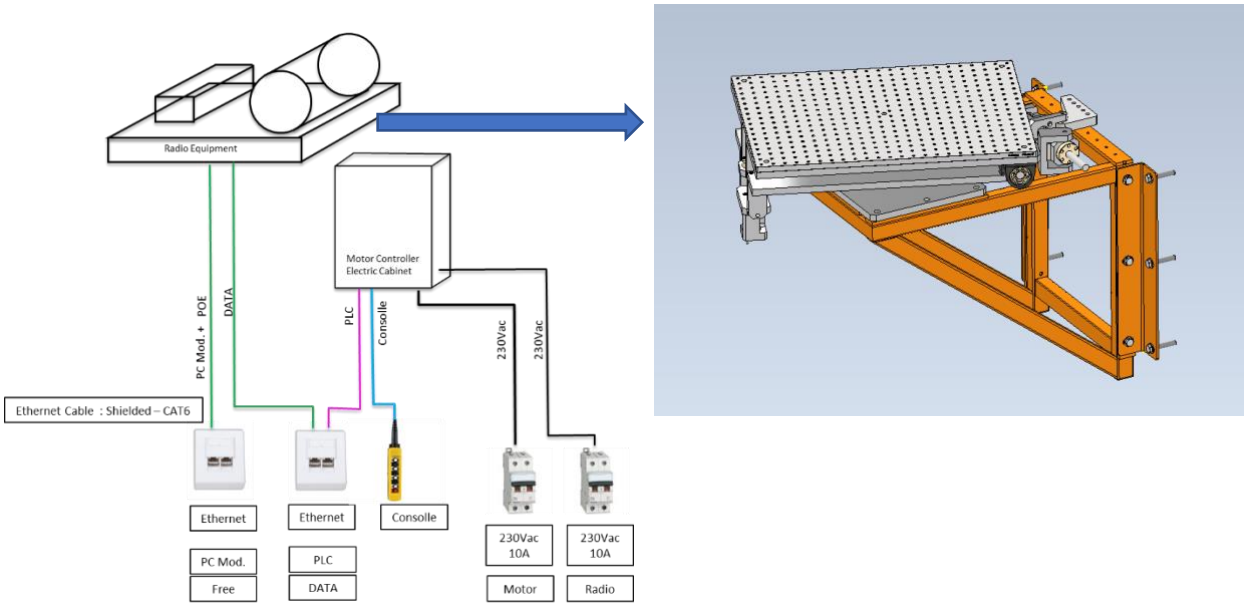

Figure 5: Short overview of the PoC1 schematics that will be installed at AETNA. Inset shows the platform 3D CAD view, that will support the radio-units and MODEMS assembled at CNRS.

2.3 Components and Equipment

The system that is built now at CNRS uses the following components:

- 2 x TIMES Indoor-Unit
- 2 x FDD-Modem (Siklu)
  - 2 x Power-over-Ethernet supplies
  - 2 x SFP cables
- 2 x WR12 diplexers
- 2 x WR3.4 diplexers
- 2 x WR12 attenuators
- 1 x WR3.4 attenuator (Only for B2B tests)
- 2 x Computers
  - USB-connection for IDUs + control software from IAF.
  - 1 Gbps Ethernet card for modems
  - 10 Gbps SFP card for modems
- 2 x High-gain antennas
- 2 x voltage generators for IDUs
- Mini PCs and EDGE Computer (industrial machines at AETNA)

2.3.1 Reflective Intelligent Surface

In the PoC-1, we will make use of the second passive RIS fabricated by Anteral, but in a panel configuration. As the first one, it was characterized in the frequency domain at CNRS. Since these results have already been discussed in the deliverable D5.4 [3], only a brief summary is provided here.

2.3.1.1 RIS bandwidth analysis by specular reflection analysis

With a 220-325 GHz VNA, performance characterization measurements were performed. First, S_{21} amplitudes are compared for RIS specular reflections and metal plate specular reflections (RS backside serving as reference) as well for different angles of arrival.

In Figure 6, we note, in the best case of $\theta_{\mathrm{AOA}} = \theta_{\mathrm{AOD}} = 34°$, that in the specular case, the RIS S_{21} only differs from metal plate between 271 GHz and 296 GHz by a clear deflecting behavior, in which the wave is reflected is a different angle than specular case. This was confirmed considering the S_{21} showing a large reduction of up to -34 dB (specular case on the mirror was -12 dB) with a 7 GHz bandwidth.

Based on this preliminary analysis of the specular behavior of the RS, the next section details the RIS bandwidth analysis of the non-specular reflection.

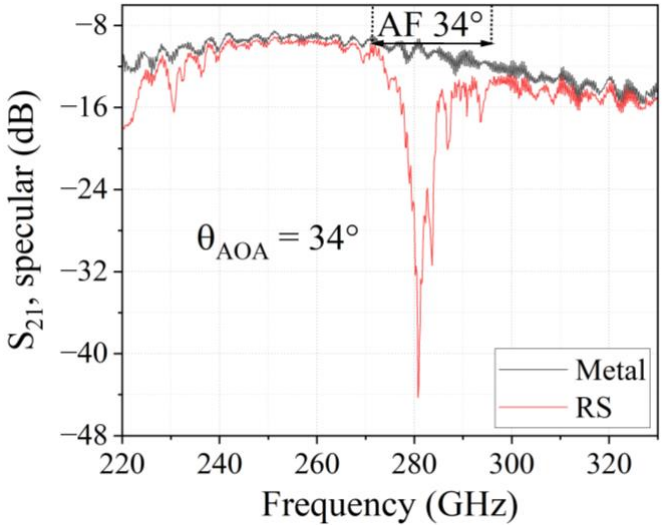

Figure 6. Example of S_{21} amplitude for specular reflection ($\theta_{AOA} = \theta_{AOD}$) configuration for the RIS (red) and for the backside metallic plate (black) for $\theta_{AOA} = 34°$.

2.3.1.2 RIS bandwidth analysis by nonspecular reflection analysis

S_{21} curves in the nonspecular case are displayed in Figure 7 and enable to compare RIS nonspecular reflections and specular reflection. Outside of the RIS bandwidth (271-296 GHz), a 60 dB decreasing is occurring, for instance, for $\theta_{\mathrm{AOA}} = 34°$ between 220 and 260 GHz. Within the RIS bandwidth, S_{21} amplitude is progressively increasing with angle of departure and reach is maximum of about -13 dB for the couple $(\theta_{\mathrm{AOA}}, \theta_{\mathrm{AOD}}) = (34°, 6°)$ at $f = 281.2$ GHz. This confirms the RIS bandwidth determined by specular configuration experiments of the previous section.

It is also important to notice that when the angles of arrival are between 20° and 30°, the maximum of S_{21} occurs at roughly $f = 287$ GHz whereas for angles of arrival between $32°$ and $44°$, it occurs at roughly $f = 281$ GHz (cf. Figure 8).

In Figure 8, the maximum of S_{21} as a function of the angle of arrival is shown for $\theta_{\mathrm{AOA}} = 34°$ at $f \approx 281$ GHz. Both maxima of S_{21} are clearly seen for $\theta_{\mathrm{AOA}} = 34°$ which corresponds to the specular case and for $\theta_{\mathrm{AOD}} = 6°$ which corresponds to the best angular configuration in the nonspecular case. We thus observe a roughly a $-30°$ shift between specular case and best nonspecular case angular configurations. More generally, when the angle θ_{AOA} is between $20°$ and $30°$, this shift is close to $+40°$ whereas for θ_{AOA} between $32°$ and $44°$ the shift is more about $-30°$. From electromagnetic simulations (performed with Floquet theory) we can conclude that $+40°$ and $-30°$ shifts are related to $n = +1$ et $n = -1$ Floquet modes, respectively.

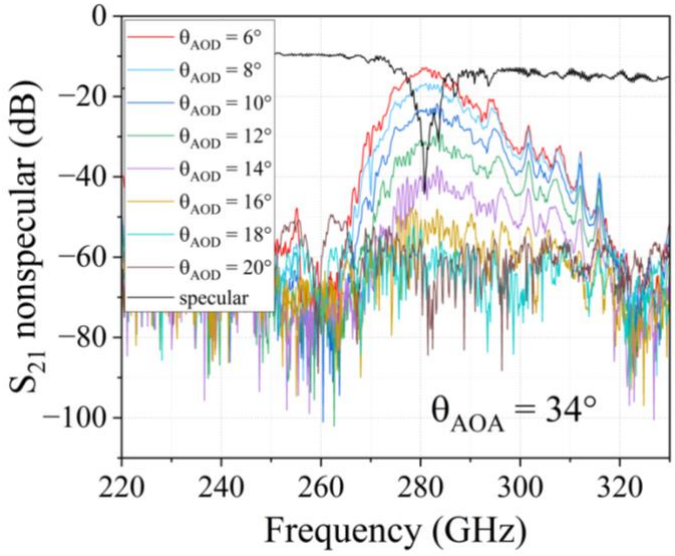

Figure 7. Comparison of S_{21} for the RIS in specular reflection (black) and nonspecular reflections (other colors) for $\theta_{AOA} = 34°$.

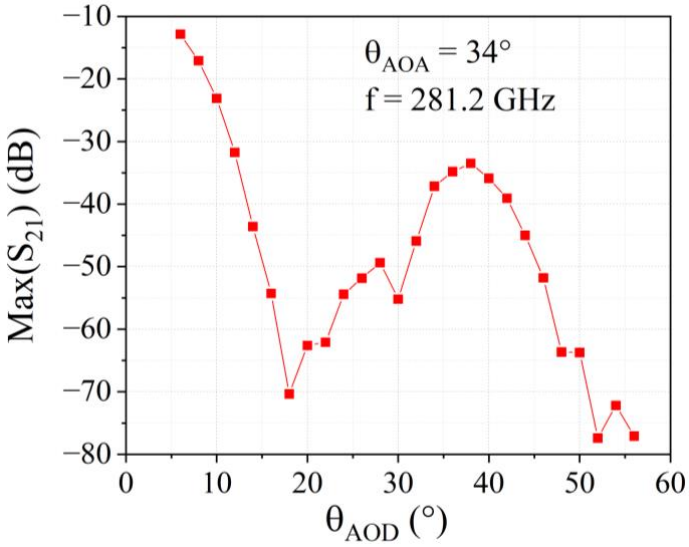

Figure 8. Evaluation of the maximum of S_{21} in terms of the angle of departure for $\theta_{AOA} = 34°$. We focused ourselves at $f = 281.2$ GHz which is the best nonspecular operation observed (maximum of S_{21}).

2.3.1.3 RIS losses determination

Figure 9 shows a zoom of the measured S_{21} specular reflection obtained with the metallic plate (RIS backside) and the maximum of S_{21} obtained for nonspecular reflection from the RIS (cf. Figure 8) between 271 and 295 GHz. The minimum losses are reached for $(\theta_{\mathrm{AOA}}, \theta_{\mathrm{AOD}}) = (34°, 6°)$ from the power difference between non-specular (from the RIS) and specular reflections (pure metallic reflector). The minimum loss induced by the RIS is thus the relative amplitude shift between the two curves. It then shows that, related to the metallic plate, the lowest RIS loss is about 1.5 dB and occurs at about 281 GHz.

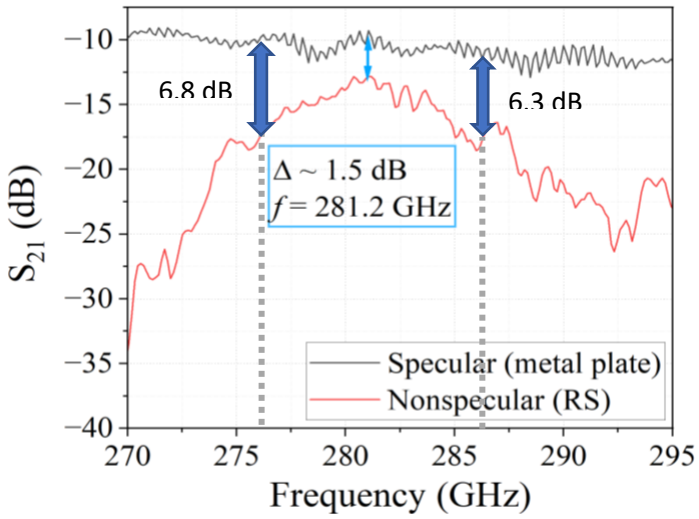

Figure 9. Zoom on the smallest measured shift between specular reflection S_{21} from the metal plate and the nonspecular reflection from the RIS which occurs for $\theta_{AOA} = 34°$ and $\theta_{AOD} = 6°$.

If we come back to the link budget calculations done previously, we can see from the Figure 9 the RIS losses that are taken into account, at 276.3 (6.8 dB) and 286.3 GHz (6.3 dB).

2.3.1.4 RIS configuration for the PoC1

According to the characterization of the RIS, the configuration shown in the Figure 10-1 has been chosen. From the setup at AETNA, 90° is angular separation between the THz propagation axis.

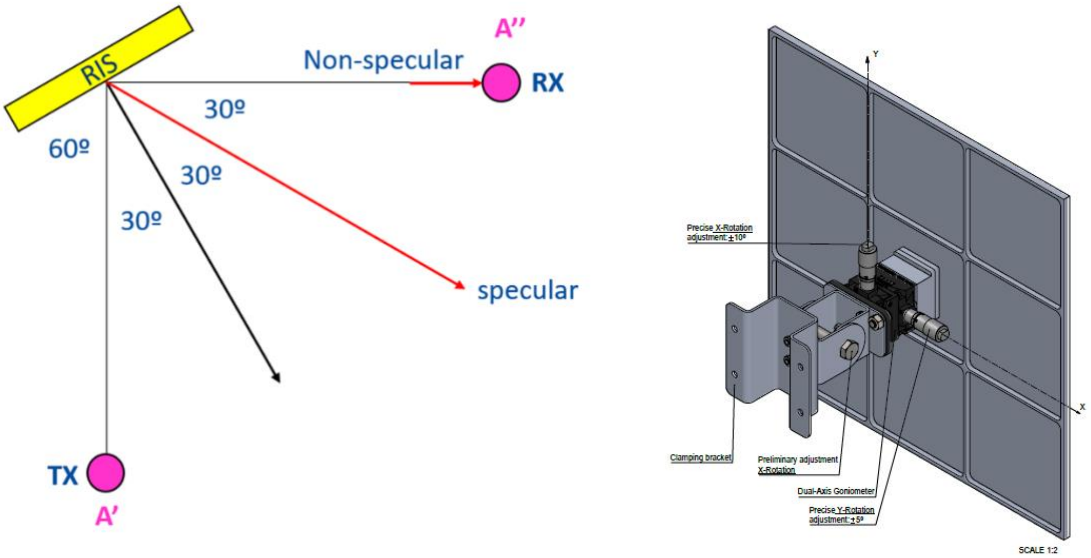

Figure 10-1. RIS configuration for PoC1. Left: the RIS is static and 90° is the angular deviation between the THz incoming signals from two sides. Right: RIS holder for PoC1.

2.3.2 Diplexer

The diplexer used in the PoC1 enables to separate at both sides the upper side band and the lower side band. This diplexer is reported in D6.2 [4]. However here we remind in Figure 10-2 the typical transfer function of one of the 2 diplexers used. The 276.3 GHz and 286.3 GHz channels are well localized in the device bandwidth.

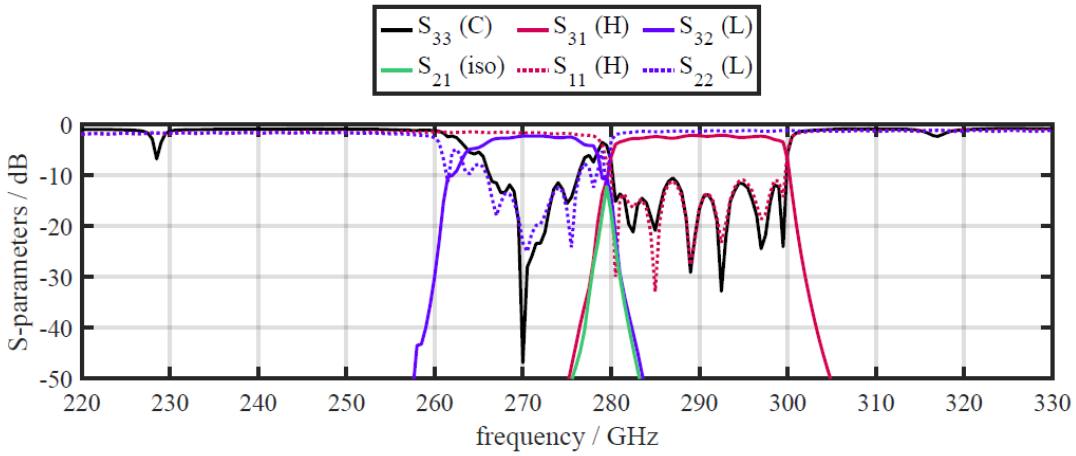

Figure 10-2. Frequency response of the diplexer (typical, here the M386-001 is shown).

2.4 Experimental Results

This work is still ongoing at the IEMN laboratory (CNRS) at this time. Thus, we present here the results already obtained that enabled to validate the link budget and the system margin ahead of the PoC1. This includes B2B measurements in WR12 and then in WR3 using IDUs. The presentation of free-space measurements with passive RIS is therefore postponed to deliverable D6.4.

2.4.1 B2B measurements in WR12

In this section, we present the first characterizations done in WR12, to check MODEMS overall link budget and range.

2.4.1.1 Setup description

For the assembly, 2 direct connections have to be established between MODEMS. To measure the system margin, a set of two variable attenuators (VA), numbered below VA1 and VA2, and four flexible waveguides (FWG), numbered below 1 to 4, are used to connect the Tx and Rx, each side.

The chosen connection for modems via FWG and VA is shown on Figure 11 (schematic) and Figure 12 (view of the assembly).

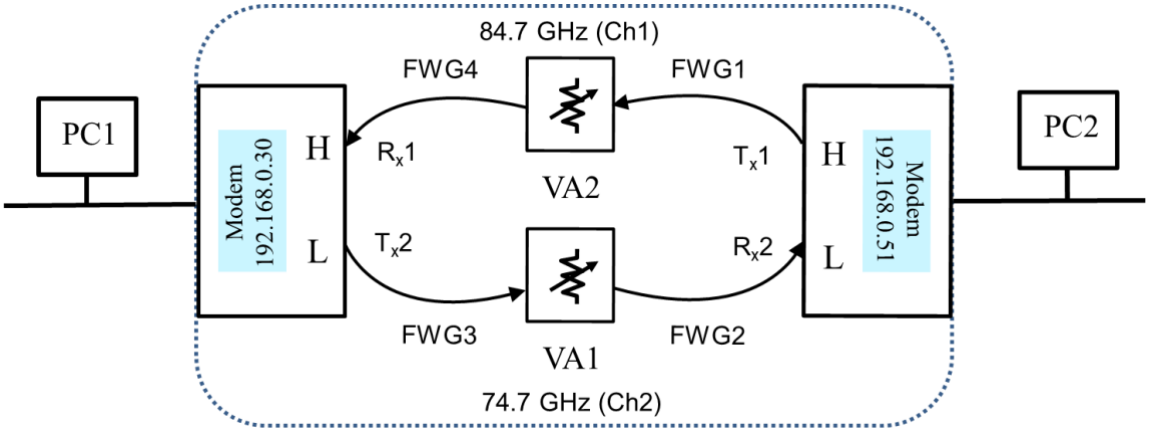

Figure 11: WR12 setup for B2B measurements: Schematic view. Dashed part is detailed by the figure 12, with photograph view.

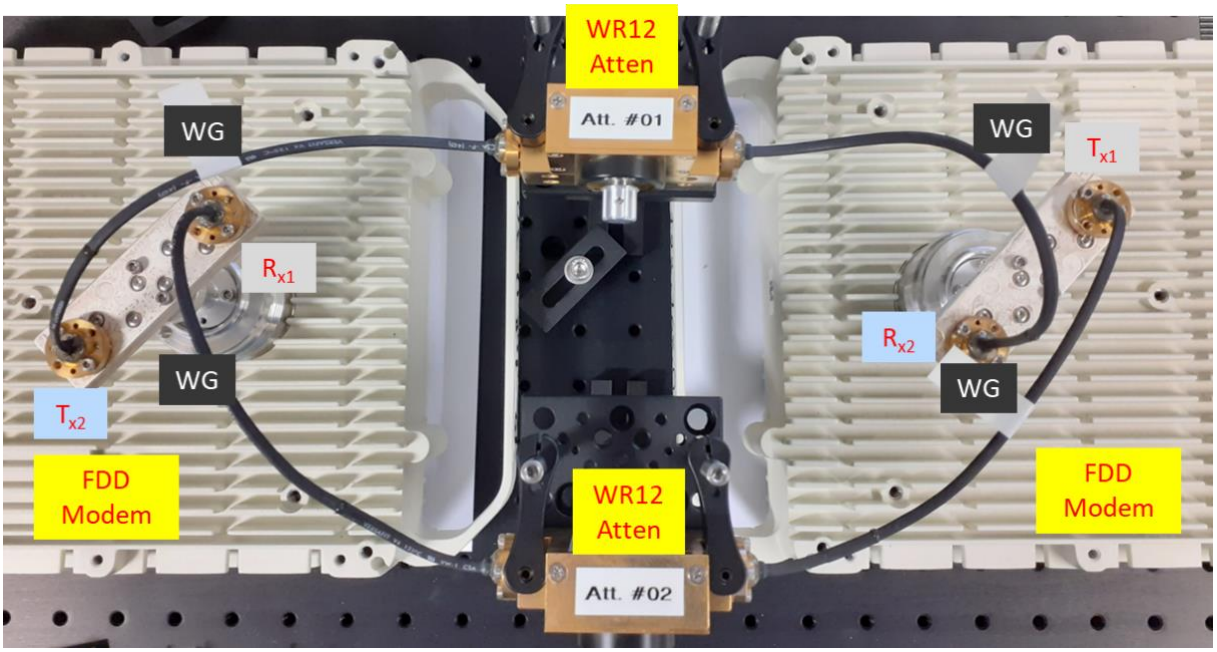

Figure 12: WR12 setup for B2B measurements: Photograph view of the MODEMS, Attenuators and flexible connections.

From this view, we can directly see the Tx and Rx positions for each modem to establish a bidirectional link at 2 carriers as part of the FDD link. As shown in Figure 11, "High" side of the modems (labeled "H" in the diagram) is associated with the 84.7 GHz frequency (Up frequency), while the "Low" side of the modems (labeled "L" in the diagram) is associated with the 74.7 GHz frequency (Down frequency), resulting in the spectra shown in the Figure 13, for WR12 and later on in WR3.

Figure 13: Frequency allocation plan WR12 (left) and WR3 (right).

For system margin measurement and optimization of the IF driving power (IDU inputs) from MODEM output, we needed to calibrate the whole RF path in waveguide. Thus, starting from the WR12 analysis (when MODEMS are directly connected to each other), we first checked the losses of the FWG connections and attenuators which is detailed in the next section.

2.4.1.2 FWG and VA characterizations

As explained previously, the first step was to characterize the FWG and the VA in the WR12 band to determine the losses in the 71-76 GHz and 81-86 GHz bands.

Regarding the FWGs, the Figure 14 shows the S_{21} for the WR12 band.

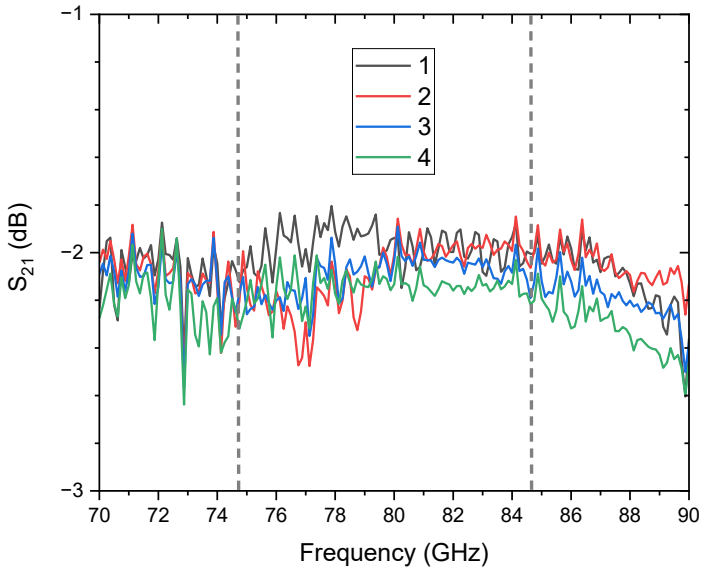

Figure 14: FWG losses in the WR12 band. The vertical bars indicate Up and Down frequencies.

This graph therefore shows us the losses of the FWGs sought:

$$@74.7\ \text{GHz} \rightarrow S_{21}^{FWG1}(74.7\ \text{GHz}) + S_{21}^{FWG4}(74.7\ \text{GHz}) = 4.6\ \text{dB}$$

$$@84.7\ \text{GHz} \rightarrow S_{21}^{FWG3}(84.7\ \text{GHz}) + S_{21}^{FWG2}(84.7\ \text{GHz}) = 4.2\ \text{dB}$$

These losses must be added to the losses induced by the VA to obtain the system's total margin in this case. For these losses, the S_{21} of the two VA was also measured, and the S_{21} value at frequencies of 74.7 and 84.7 GHz is plotted as a function of possible attenuation values in Figure 15:

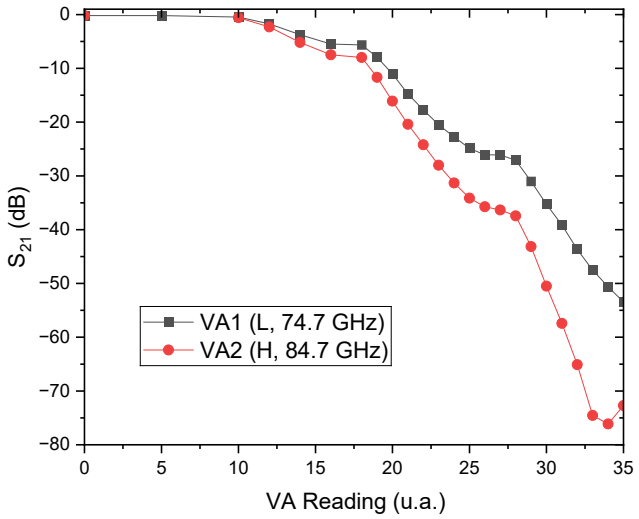

Figure 15: Attenuation given by VA at Up and Down frequencies (H and L), for E-band MODEM system margin measurements..

2.4.1.3 CINR, RSSI and data-rate measurements in WR12

2.4.1.3.1 Siklu interface and IPERF

The Figure 16 below shows the Siklu interface of a modem when the link is active.

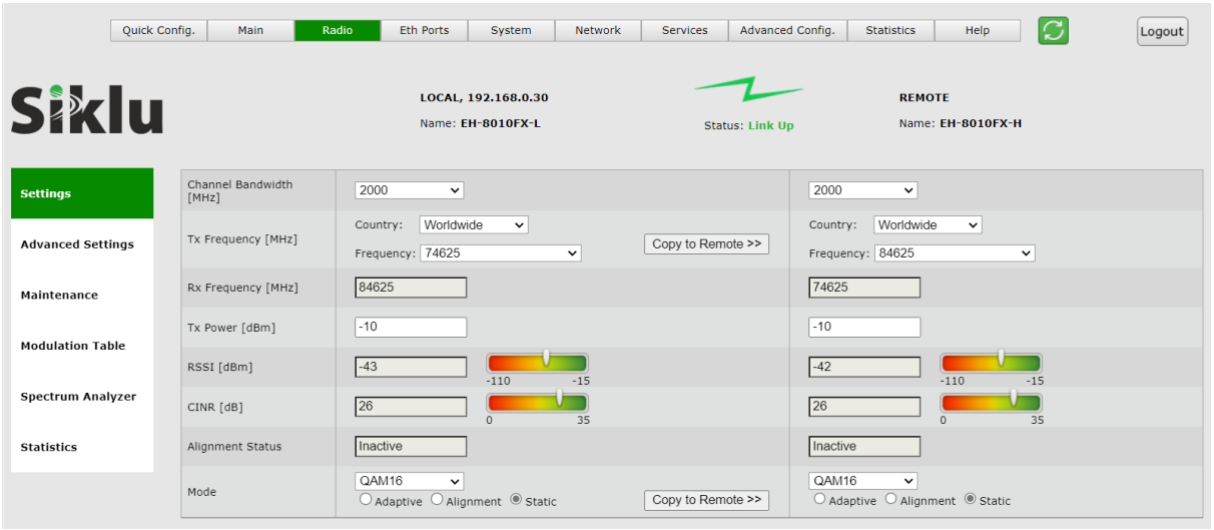

Figure 16: Siklu web interface to drive modems. The MODEM are controlled using the 1 Gbps Ethernet port.

On the web interface, when the link is up and running, we then see the two modems RSSI and CINR, related to the two links. This display shows the "Local" modem, that is, the one connected to the PC on which we are

viewing the interface, with its IP address, and the "Remote" modem, which is the second modem. We also see the frequencies of T_{x1}, T_{x2}, R_{x1}, and R_{x2}, as shown in the previous diagram.

Below is the Tx power on each side (here equal to -10 dBm). When describing the power measurements, this value will be varied, but for now, we will assume a constant P_{Tx}. Finally, we find the RSSI (in dBm), the CINR (in dB), and the chosen modulation (here, QAM-16) for both modems. It is important to note that we are using "Static" modulation here to determine the values of these metrics for each tested modulation: QPSK (QPSK3 in the interface), QAM-16, QAM-32, and QAM-64.

The last metric to measure is data-rate via IPERF, which is used through the command prompt. The Figure 17 shows the possible IPERF commands:

```
C:\Users\THz-admin-local\Desktop\iperf-3.1.3-win64>iperf3.exe
iperf3: parameter error - must either be a client (-c) or server (-s)

Usage: iperf [-s|-c host] [options]
       iperf [-h|--help] [-v|--version]

Server or Client:
  -p, --port      #         server port to listen on/connect to
  -f, --format    [kmgKMG]  format to report: Kbits, Mbits, KBytes, MBytes
  -i, --interval  #         seconds between periodic bandwidth reports
  -F, --file name           xmit/recv the specified file
  -B, --bind      <host>    bind to a specific interface
  -V, --verbose             more detailed output
  -J, --json                output in JSON format
  --logfile f               send output to a log file
  -d, --debug               emit debugging output
  -v, --version             show version information and quit
  -h, --help                show this message and quit
Server specific:
  -s, --server              run in server mode
  -D, --daemon              run the server as a daemon
  -I, --pidfile file        write PID file
  -1, --one-off             handle one client connection then exit
Client specific:
  -c, --client    <host>    run in client mode, connecting to <host>
  -u, --udp                 use UDP rather than TCP
  -b, --bandwidth #[KMG][/#] target bandwidth in bits/sec (0 for unlimited)
                            (default 1 Mbit/sec for UDP, unlimited for TCP)
                            (optional slash and packet count for burst mode)
  -t, --time      #         time in seconds to transmit for (default 10 secs)
  -n, --bytes     #[KMG]    number of bytes to transmit (instead of -t)
  -k, --blockcount #[KMG]   number of blocks (packets) to transmit (instead of -t or -n)
  -l, --len       #[KMG]    length of buffer to read or write
                            (default 128 KB for TCP, 8 KB for UDP)
  --cport         <port>    bind to a specific client port (TCP and UDP, default: ephemeral port)
  -P, --parallel  #         number of parallel client streams to run
  -R, --reverse             run in reverse mode (server sends, client receives)
  -w, --window    #[KMG]    set window size / socket buffer size
  -M, --set-mss   #         set TCP/SCTP maximum segment size (MTU - 40 bytes)
  -N, --no-delay            set TCP/SCTP no delay, disabling Nagle's Algorithm
  -4, --version4            only use IPv4
  -6, --version6            only use IPv6
  -S, --tos N               set the IP 'type of service'
  -Z, --zerocopy            use a 'zero copy' method of sending data
  -O, --omit N              omit the first n seconds
  -T, --title str           prefix every output line with this string
  --get-server-output       get results from server
  --udp-counters-64bit      use 64-bit counters in UDP test packets

[KMG] indicates options that support a K/M/G suffix for kilo-, mega-, or giga-

iperf3 homepage at: http://software.es.net/iperf/
Report bugs to:     https://github.com/esnet/iperf
```

Figure 17: All IPERF possible prompts.

and the Figure 18 shows an example of flow measurement via IPERF in QAM-16 with the associated command to type:

```
C:\Users\THz-admin-local\Desktop\iperf-3.1.3-win64>iperf3 -c 192.168.0.12 -w 4m -bidir
Connecting to host 192.168.0.12, port 5201
[  4] local 192.168.0.13 port 49851 connected to 192.168.0.12 port 5201
[ ID] Interval           Transfer     Bandwidth
[  4]   0.00-1.00   sec   612 MBytes  5.14 Gbits/sec
[  4]   1.00-2.00   sec   617 MBytes  5.17 Gbits/sec
[  4]   2.00-3.00   sec   616 MBytes  5.17 Gbits/sec
[  4]   3.00-4.00   sec   614 MBytes  5.15 Gbits/sec
[  4]   4.00-5.00   sec   617 MBytes  5.18 Gbits/sec
[  4]   5.00-6.00   sec   614 MBytes  5.15 Gbits/sec
[  4]   6.00-7.00   sec   617 MBytes  5.18 Gbits/sec
[  4]   7.00-8.00   sec   617 MBytes  5.17 Gbits/sec
[  4]   8.00-9.00   sec   617 MBytes  5.18 Gbits/sec
[  4]   9.00-10.00  sec   617 MBytes  5.18 Gbits/sec
- - - - - - - - - - - - - - - - - - - - - - - - -
[ ID] Interval           Transfer     Bandwidth
[  4]   0.00-10.00  sec  6.01 GBytes  5.17 Gbits/sec                  sender
[  4]   0.00-10.00  sec  6.01 GBytes  5.17 Gbits/sec                  receiver

iperf Done.
```

Figure 18: Typical flow measurement via IPERF in QAM-16.

The IP address 192.168.0.12 does not correspond to one of the modems (shown in the previous diagram) but to the IP address of the SFP module of one of the modems. Each modem has two connection outputs, as shown in the interface diagram at the top. The first is an RJ45 output, used for both power via PoE and data transfer, but at a maximum speed of 1 Gbps. The second is an SFP output (optical port), which allows data transfer at a maximum speed of 10 Gbps. It is this second output that we are interested in here.

Here, during the tests, the SFP IP address of modem 192.168.0.51 is 192.168.0.12, and the SFP IP address of modem 192.168.0.30 is 192.168.0.13 (these IP addresses were chosen arbitrarily as long as they did not conflict with another address). It's also important to note that the first few numbers in the 192.168.0.xx range must be identical to be placed in the same subnet. They must also have the same subnet mask and gateway.

Thus, in the image above, a modem is forced to act as a server by typing `iperf3 -s` on the corresponding PC, and data can then be sent to the SFP card of the remote PC (the client) by typing `-c [SFP card IP address of remote PC] -w 4m -bidir`. We can see that for 10 seconds, packets of approximately 617 Mbps were transmitted each second, with a data-rate of about 5.17 Gbps. It is important to specify 1) that both PCs display this window but with the data sent or received, therefore potentially different, 2) that the server PC is always active and that you will need to type the combination `ctrl+c` on the keyboard to interrupt the command and 3) that it is not necessary to have the Siklu interfaces connected to run IPERF.

2.4.1.3.2 CINR, RSSI and data-rate measurements in WR12

CINR (Carrier to Interference and Noise Ratio) corresponds to the signal-to-noise ratio, taking into account interferences present on the whole chain. RSSI corresponds to the power received by each modem, and the data-rate corresponds to the number of data points transferred between the two PCs via the modems per second. These different metrics were therefore measured for various attenuation levels to determine their minimum values for an active link between the two modems.

As the attenuation is decreased, four different situations can occur.

1) When the attenuation is too high, the CINR and RSSI are not measurable, and the web interface simply displays a value of -128 for both. This is just to show that it is not measurable without any physical reality.

2) When the attenuation is slightly less severe, the Link is still Down, but the CINR and RSSI of both modems are still measurable (ie in the range of values detected by the MODEM). The web interface displays a physical value for both even though the data-rate is not measurable.
3) For higher-order modulations such as QAM-32 or QAM-64, the CINR may be too low for the data rate to be sufficient. In this case, the link is indeed up, the web interface displays correct physical values for CINR and RSSI, but the data rate is 0 Gbps.
4) The attenuation is not too high, the Link is Up, the CINR and RSSI are correct and high enough to have a non-zero data-rate. This is the ideal case we aim for.

For the measurements themselves, modem 30 was chosen as the server (S) and modem 51 as the client (C). Therefore, in this case, channel 1 (Ch1) is defined as Tx1 to Rx1, i.e., 30 (S) and 51 (C), and channel 2 (Ch2) as Tx2 to Rx2, i.e., 51 (S) and 30 (C), which is the reverse path to verify the symmetry of the two channels. The CINR, RSSI, and data rate were measured for four different modulation schemes: QPSK, QAM-16, QAM-32, and QAM-64/QAM-128 depending on the case (high CINR available).

Then, we plot on the same graph:

- CINR vs Loss (Ch1) (Ch1_CINR_Loss)
- CINR vs Loss (Ch2) (Ch2_CINR_Loss)
- CINR vs RSSI (Ch1) (Ch1_CINR_RSSI)
- CINR vs RSSI (Ch2) (Ch2_CINR_RSSI)
- Data-rate (Ch1) vs total losses (Ch1_DR_Loss)
- Data-rate (Ch2) vs total losses (Ch2_DR_Loss)

For QPSK modulation, we find the results shown in the Figure 19:

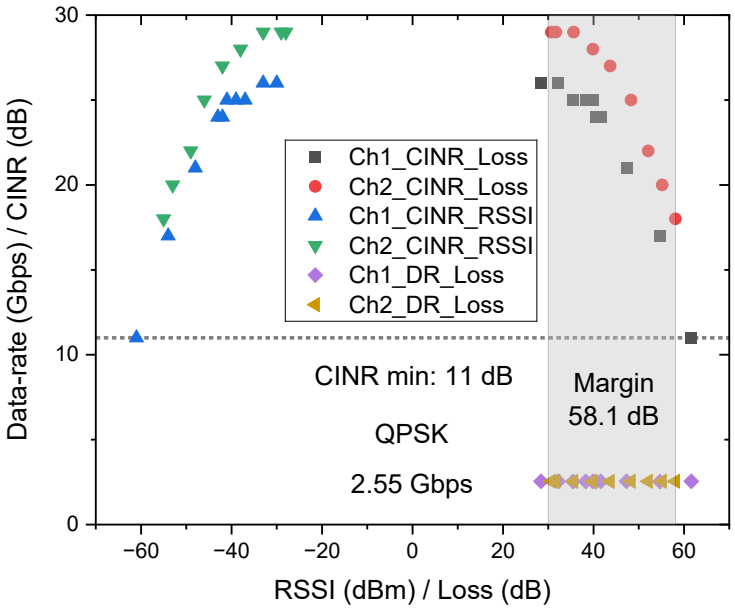

Figure 19: QPSK performance measurements in WR12. In the grey region, the 2 channels are up and FDD is running. The margin is defined as the maximum possible attenuation set between the Tx and the Rx.

The general trends are clearly visible for each of the measured quantities. As expected, the performances increase when loss is lower than a certain limit. Up to close to 60 dB, the link was up for both channels. Values

are detailed in the Table 1. The system margin (i.e. the maximum losses between Tx and Rx is the maximum loss on which both channels are operating, i.e. FDD operation is up and running.

		RSSI Min	CINR Min	Data-rate (DR)	Margin
		dBm	dB	Gbps	dB
QPSK	Ch1	-61	11	2.55	61.6
QPSK	Ch2	-55	18	2.55	58.1

Table 1: Minimum performances to get a Link Up (QPSK modulation) in WR12.

For QAM-16 modulation, the same tests were done, and Figure 20 presents the outcome of these measurements:

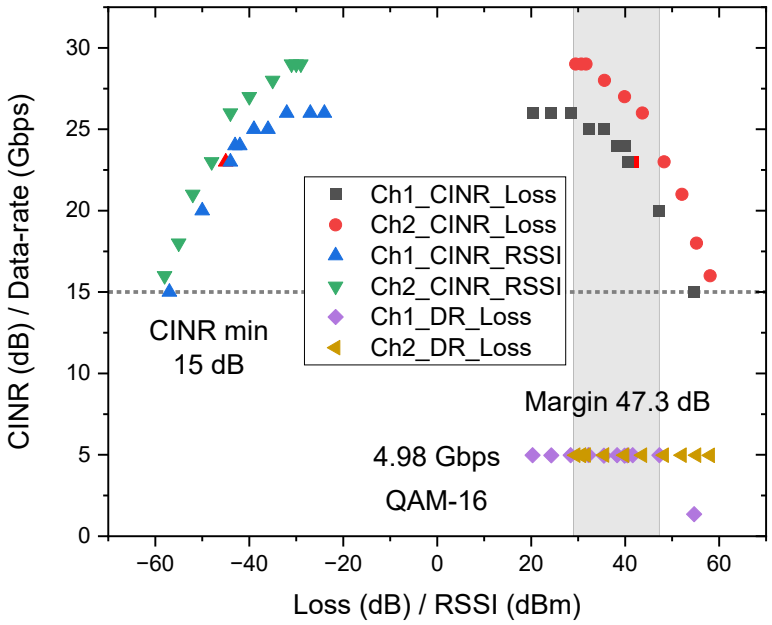

Figure 20: QAM-16 performance measurements in WR12.

The associated Table 2 for a Link "Up", i.e. when the data-rate measured via IPERF is what is expected from the QPSK test. Here the available DR is doubled, and the margin smaller.

		RSSI Min	CINR Min	Data-rate (DR)	Margin
		dBm	dB	Gbps	dB
QAM-16	Ch1	-50	20	4,98	47.3
QAM-16	Ch2	-55	18	4.98	55.2

Table 2: Minimum performances to get a Link Up (QAM-16 modulation) in WR12.

For QAM-32 modulation, it comes down to the Figure 21:

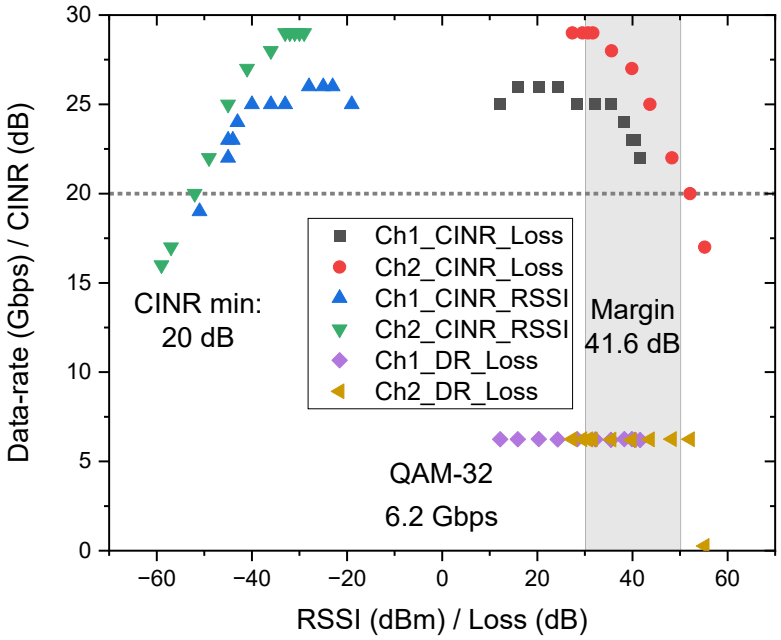

Figure 21: QAM-32 performance measurements in WR12. Margin is 41.6 dB to get two channel up.

The Link Up Table 3 shows:

		RSSI Min	CINR Min	Data-rate (DR)	Margin
		dBm	dB	Gbps	dB
QAM-32	Ch1	-45	22	6.2	41.6
QAM-32	Ch2	-52	20	6.24	52.1

Table 3: Minimum performances to get a Link Up (QAM-32 modulation) in WR12.

Going towards the highest possible modulations, QAM-64 and QAM-128, the tests were possible with expected margin reduction. QAM-64 and QAM-128 performances are shown in Figure 22.

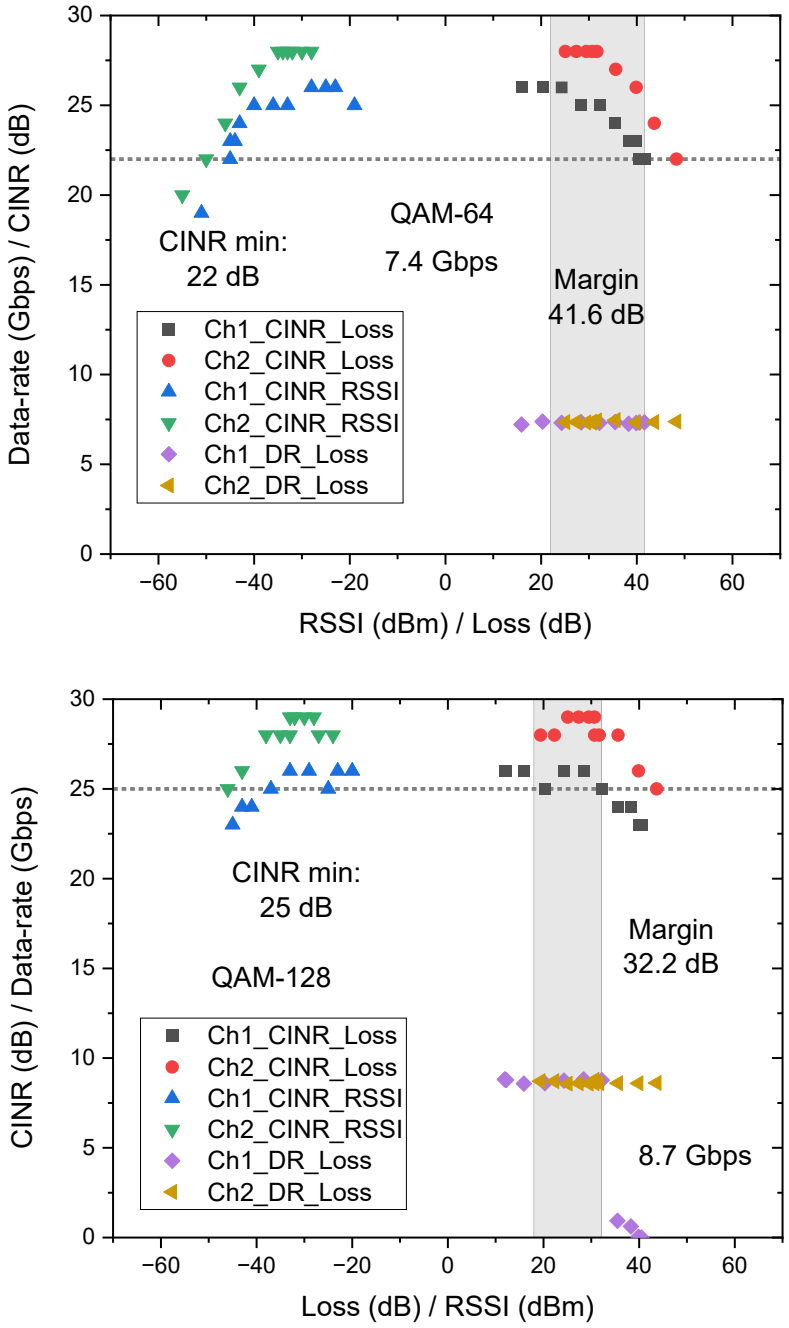

Figure 22: QAM-64 and QAM-128 performance measurements in WR12.

The Link Up Table 4 shows the margin for these last 2 modulations.

		RSSI Min	CINR Min	Data-rate (DR)	Margin
		dBm	dB	Gbps	dB
QAM-64	Ch1	-47	22	7.34	41.6
QAM-64	Ch2	-50	22	7.38	48.3
QAM-128	Ch1	-37	25	8.7	32.2
QAM-128	Ch2	-46	25	8.7	43.7

Table 4: Minimum performances to get a Link Up (QAM-64 and QAM-128 modulation) in WR12.

Depending on the different modulations, several things can be observed:

- An increasingly RSSI is needed to achieve a Link Up.
- The same applies to the CINR, as could be expected from Shannon theorem. From QPSK to QAM-128, the required minimal CINR to operate the link is more and more demanding.
- As a consequence, the data-rate / system margin evolves accordingly, ie highest data-rates come with a reduced margin and a more demanding system performance (as in linearity).

2.4.1.3.3 Comparisons for the different modulations

From the measurements, the minimum margin for each modulation I determined for both channels:

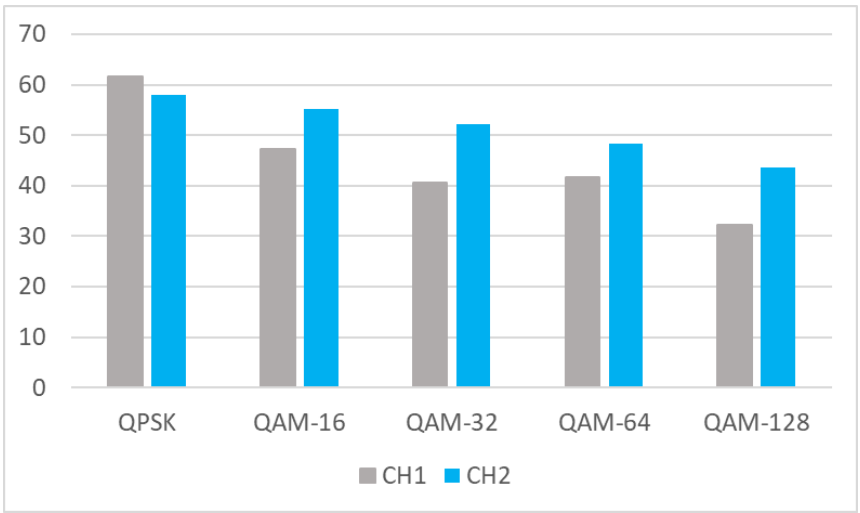

Figure 23: Available system margin for each modulation formats in WR12 band.

This graph shows several things:

- The higher the modulation, the lower the margin, which is consistent.

- For Ch2, for QAM-16, QAM-32, QAM-64 and QAM-128 modulations, the margin is lower than for Ch1, that can come from the MODEM performances and linearity. Surely related to internal losses not taken into account.

Regarding this graph, it is important to note that we are still in the WR12 band, not WR3. It is then worth to remind that the margin will be even smaller at 300 GHz. For this reason, we decided to exclude QAM-64 and QAM-128 from the subsequent analysis.

2.4.1.4 Tx linearity

The final measurements to be taken in WR12 concern the linearity of the output power as a function of the Tx power, to optimize the input power incoming to the TIMES outdoor units (IF side). Maintaining linearity also helps to avoid transmitter saturation problems and constellation distortions, particularly for higher orders.

To do this, we use the Erickson PM5B VDI to measure the power at Tx outputs. An analysis for P_{Tx1} and P_{Tx2} between -10 and +10 dBm for all modulations between QPSK and QAM-128 and for an attenuation of 0 dB. We then obtain the figure 24.

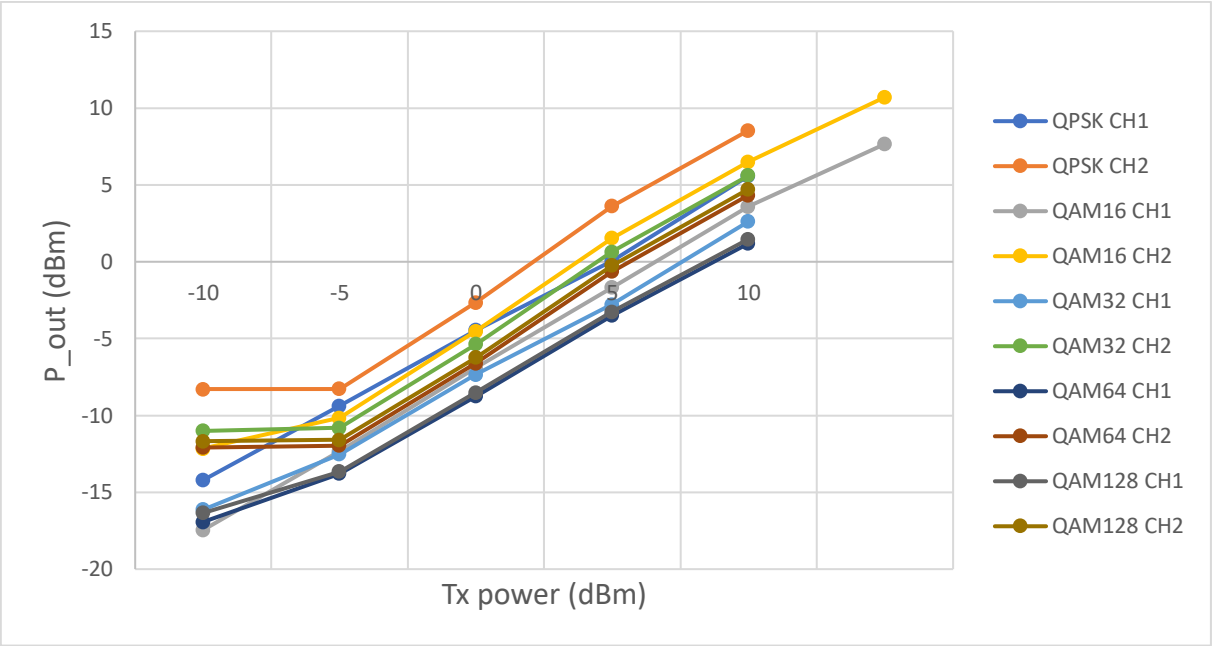

Figure 24: Tx linearity in WR12.

We can then see that P_{Rx} remains linear regardless of P_{Tx} between -10 and 10 dBm.

2.4.2 B2B measurements in WR3

After validation of the B2B measurements carried out in the WR12 band, we move on to the B2B measurements carried out in the WR3 band (220-325 GHz) via the IDUs provided by Fraunhofer IAF.

2.4.2.1 Description and operation of IDUs

These IDUs require power to operate. A 6V and 3.2A compliance current are necessary to ensure proper module function. In this case, the IDUs can be connected to PCs via a COM port for control through a software interface. This interface is shown in the figure 25:

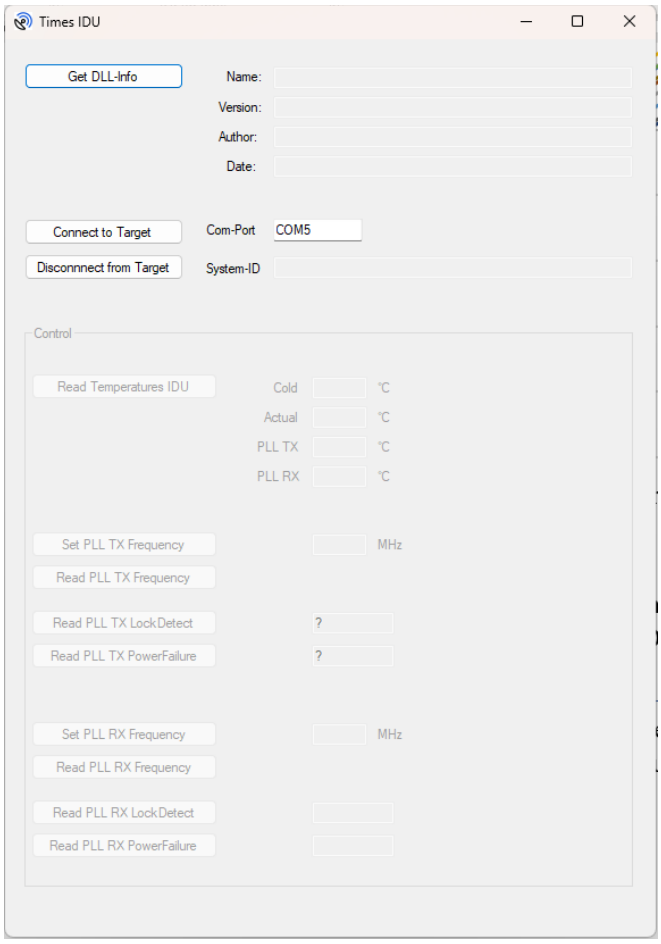

Figure 25: IDU software interface.

This interface allows to read and modify the frequencies chosen for the PLL, the Tx, and the Rx. According to deliverable D6.2, the optimal PLL frequency is 25.2 GHz, so we set it to this value to perform initial linearity measurements of the two modules, one by one. For CH1, the chosen IDU is IDU 4, and for CH2, it is IDU 3.

For adapting the setup with the IDUs, refer to Figure 26:

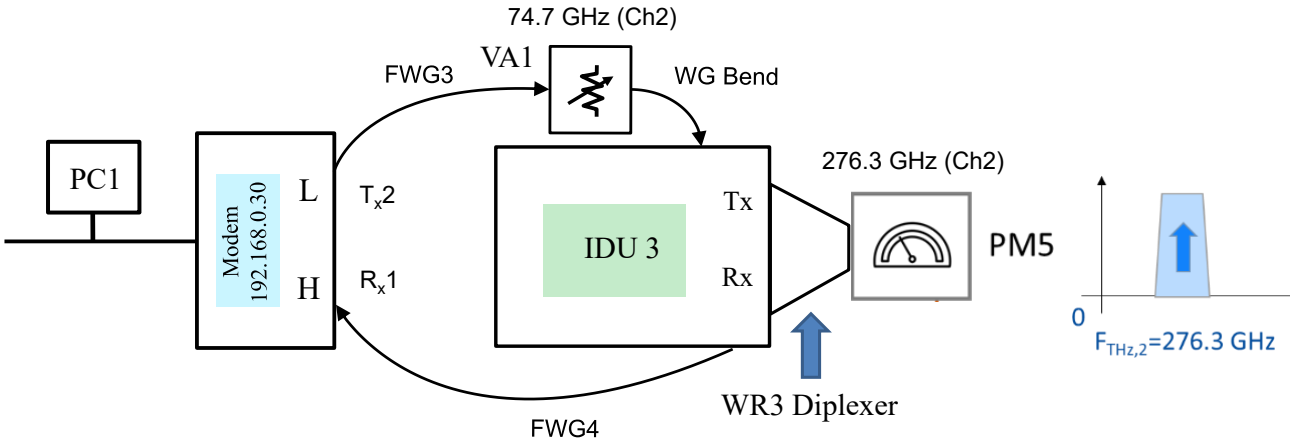

Figure 26: Setup of IDU characterization measurements in WR3: measurement of Ch2 (74.7 GHz in WR12, 276.7 GHz after up-conversion in the 300 GHz band.

In this diagram, the PC and the modem are still connected by SFP cable and the FWGs are also present as the VA 1. However, now the FWGs are attached to the IDUs and the diplexer allow data to be sent bidirectionally for the final assembly with the second IDU and Tx1, Rx2 and second MODEM.

As mentioned previously, before any connection between the two modules, they must be characterized, and in particular, their linearity in the Tx direction must be tested. Figure 27 is the outcome of this test:

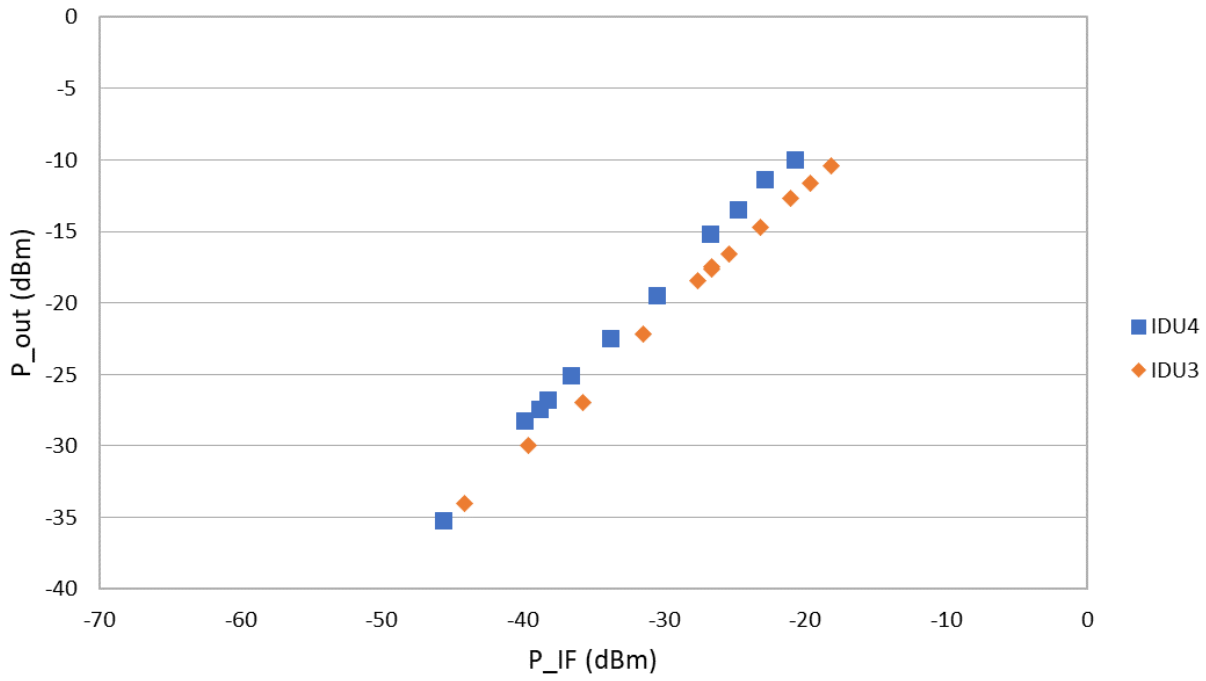

Figure 27: Tx linearity of IDUs: P_IF is a signal in WR12, while P_out is in WR3 band.

From P_{Tx} set, we obtain the actual output power, taking into account the losses due to FWG for each channel. We then set $P_{\mathrm{Tx}} = 0$ dBm for better linearity and obtain the IF power at IDU input (IF-in) using the relation

$$P_{\mathrm{IF}} = P_{\mathrm{Tx}}^{\mathrm{FWG3}} + S_{21}^{\mathrm{VA1}} + S_{21}^{\mathrm{WG-bend}}$$

This is the actual output power of the WR12 diplexer (L-side) minus the impact of the VA and FWG that connect the modem to the IDU.

We can then see that the graph is indeed linear for both modules, while keeping IF-in lower than -20 dBm. This curve is in line with the performance of the modules provided by Fraunhofer IAF. Another interesting metric is the conversion gain, which is given by:

$$G_{\mathrm{c}} = P_{\mathrm{out}} - P_{\mathrm{IF}}.$$

In our case, for both modules, for different modulations and for the same PLL frequency of 25.2 GHz, we find a conversion gain of about 11-12 dB for IDU4 and 8-9 dB for IDU3 (including the diplexer), in line with expected specifications from IAF.

Finally, measurements are carried out to characterize the diplexer by varying the PLL frequency. For IDU 3 and for an attenuation which corresponds to $P_{\mathrm{Tx2}}\ (f_{PLL} = 25.2\ \mathrm{GHz}) = -17$ dBm (in QPSK) which was used to stay in the linear regime, and by setting the PLL frequency between 24.4 and 25.6 GHz since these frequencies are within the module's available range. In this case, the RF frequency is written

$$f_{RF} = 8f_{PLL} + f_{\mathrm{Tx}}, [4]$$

Since $f_{\mathrm{Tx2}} = 74.7$ GHz, f_{RF} varies between 269.8 and 279.4 GHz. The Figure 28 shows the output power as a function of the RF frequency:

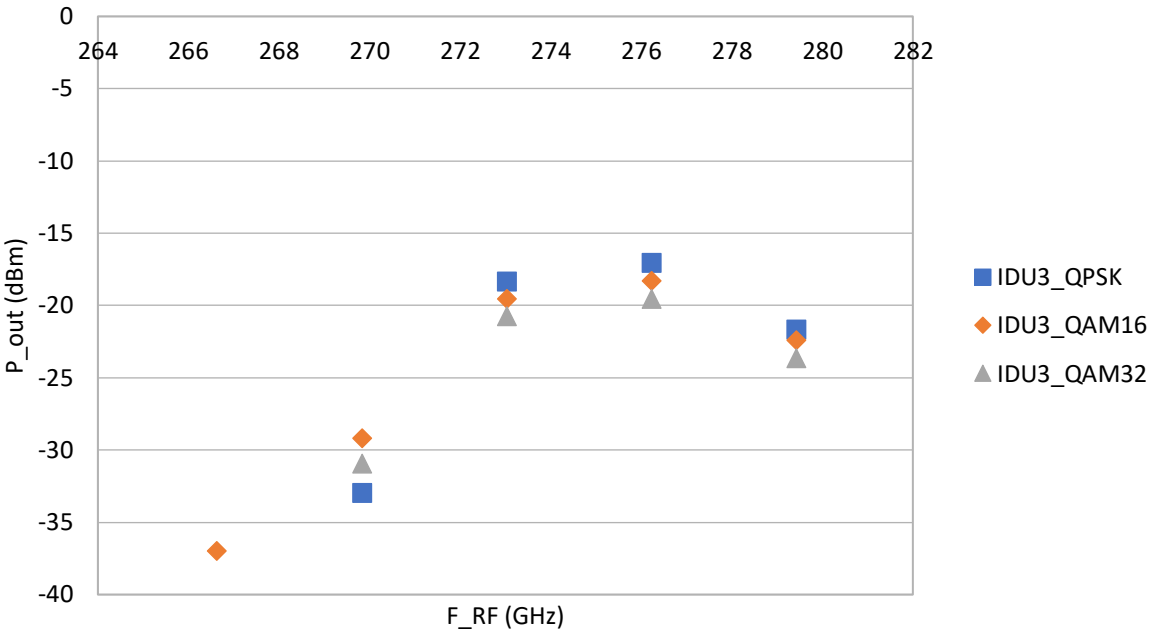

Figure 28: Output power frequency response as per configuration of figure 26.

Figure 28 should be compared with Figure 9 of deliverable D6.2 [4]. The maximum power is -17 dBm in QPSK and is found at a frequency of 276.2 GHz.

The same applies to IDU 4. This time, we set the attenuation such that $P_{\mathrm{Tx1}}(f_{PLL} = 25.2\ GHz) = -15$ dBm (in QPSK). We varied the PLL frequency between 24 and 27.2 GHz, which corresponds to an RF frequency between 276.6 and 302.2 GHz, and we found the Figure 29:

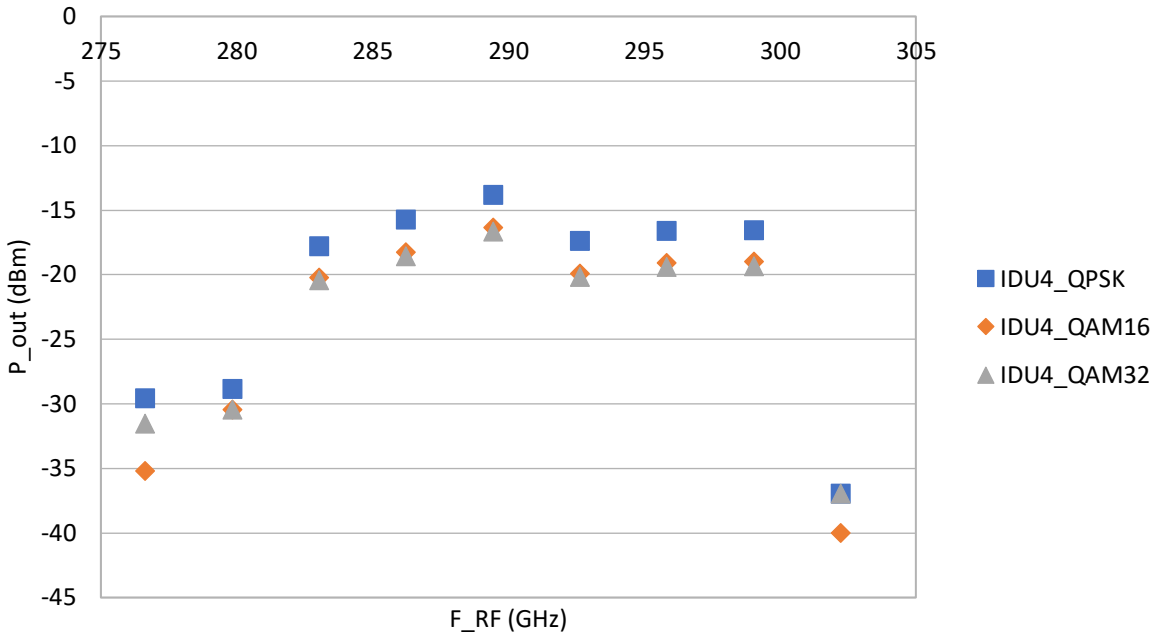

Figure 29: Diplexer characterization in the view of Up frequency.

The results of Figure 29 should be compared with Figure 8 of deliverable D6.2 [4]. This time, the maximum power is -13.8 dBm at a frequency of 289.4 GHz. Therefore, the central frequency is 282.8 GHz, very close to the optimal frequency for passive RIS, which is 281.2 GHz. Then for now, in QPSK, QAM-16 and QAM-32, IDUs seem to work as expected. The next step is the characterization of IDUs in the back-to-back, WR3.

2.4.2.2 CINR, RSSI and data-rate measurements in WR3

Eventually, we connected both modules to obtain the setup shown in Figure 30:

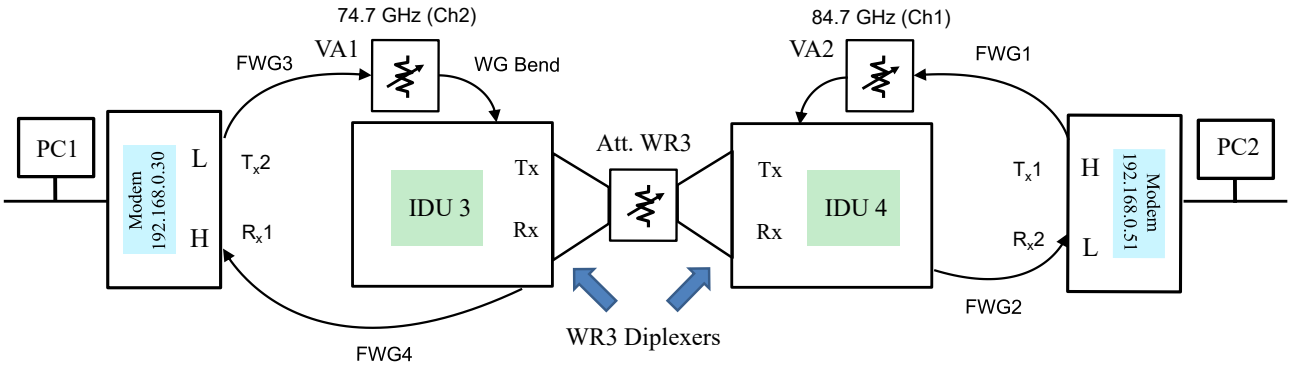

Figure 30: Setup of B2B measurements in WR3.

A new VA (VA3) is installed to simulate the pathloss between the two modules and the goal is to find the minimum attenuation to have a Link Up for each modulation formats in terms of CINR, RSSI and data-rate as before (in WR12 band) but this time in WR3 band.

As before, web interface of modems is used to measure each metrics as a function of VA3 losses, that was calibrated using a VNA ahead of the measurements. Therefore, it is necessary to characterize this new VA first, typical attenuation range is shown in the figure 31.

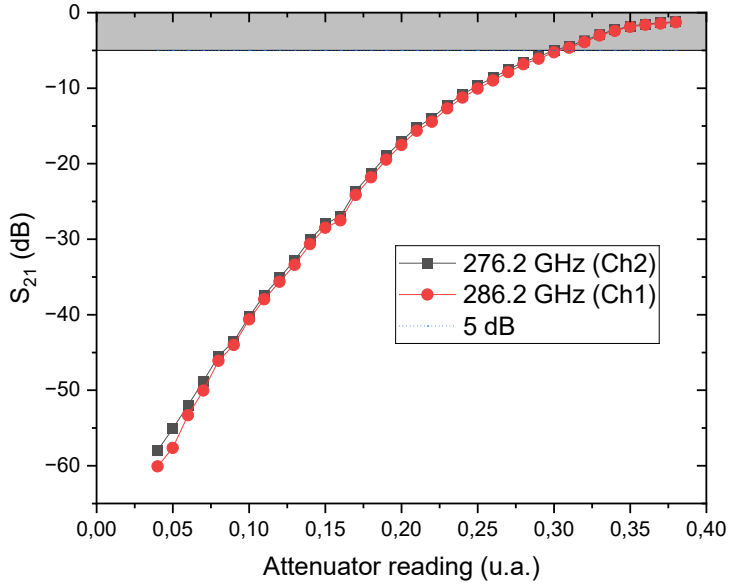

Figure 31: Amount of attenuation for VA3 at RF frequencies of interest. The -5 dB line illustrates the limit that must not be exceeded to avoid damaging the IDUs. The attenuator available range enabled to go to a position where the link was "down".

We measured the minimum performances for QPSK, QAM-16 and QAM-32 modulations since for QAM-64, the CINR was too low to have a link Up. Figure 32 shows link performances for QPSK, summarized in Table 5.

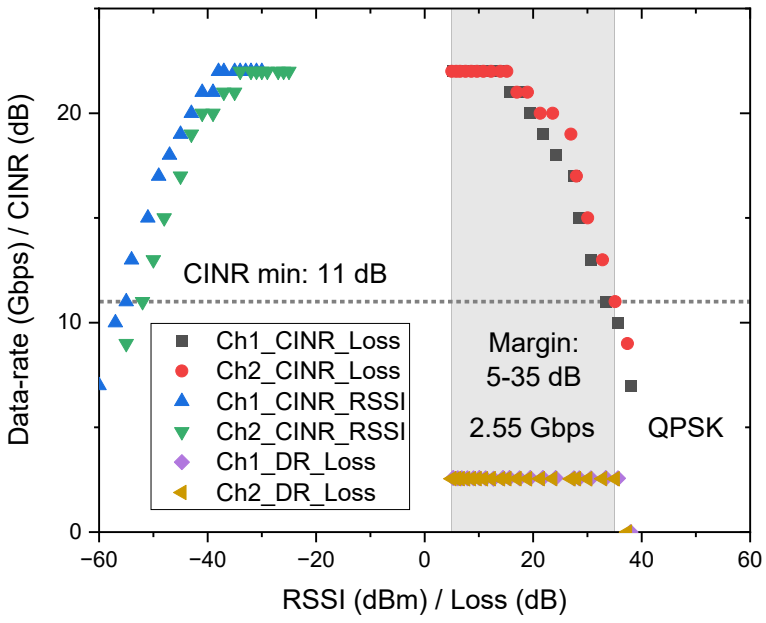

Figure 32: QPSK performance measurements in WR3, where system margin is 35 dB

		RSSI Min	CINR Min	Data-rate (DR)	Margin
		dBm	dB	Gbps	dB
QPSK	Ch1	-57	10	2.57	35.6
QPSK	Ch2	-52	11	2.54	35.1

Table 5: Minimum performances to get a Link Up (QPSK modulation) in the 300 GHz band (WR3).

For QAM-16, the Figure 33 shows the obtained performance and associated margin.

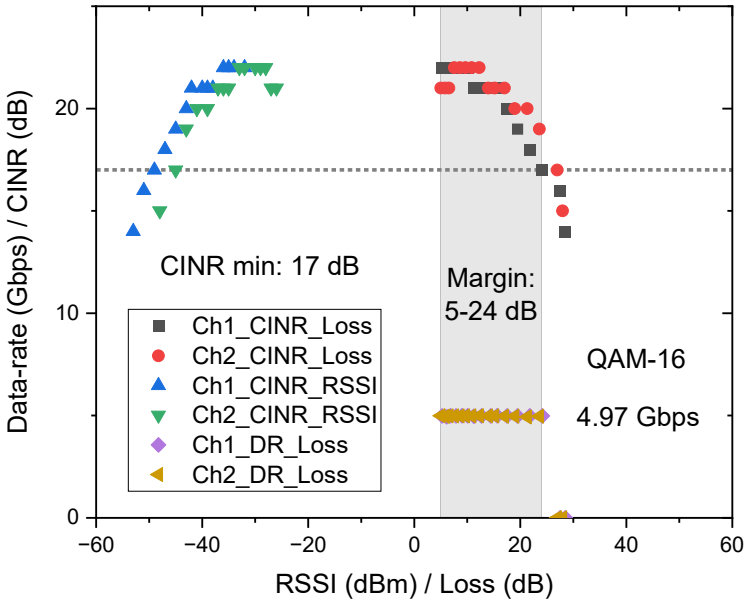

Figure 33: QAM-16 performance measurements in WR3. System margin is 24 dB.

The Table 6 below summarizes the QAM-16 performances and margin.

		RSSI Min	CINR Min	Data-rate (DR)	Margin
		dBm	dB	Gbps	dB
QAM-16	Ch1	-49	17	4.98	24.1
QAM-16	Ch2	-43	19	4.97	23.6

Table 6: Minimum performances to get a Link Up (QAM-16 modulation) in WR3.

For QAM-32, the Figure 34 shows the measured performances.

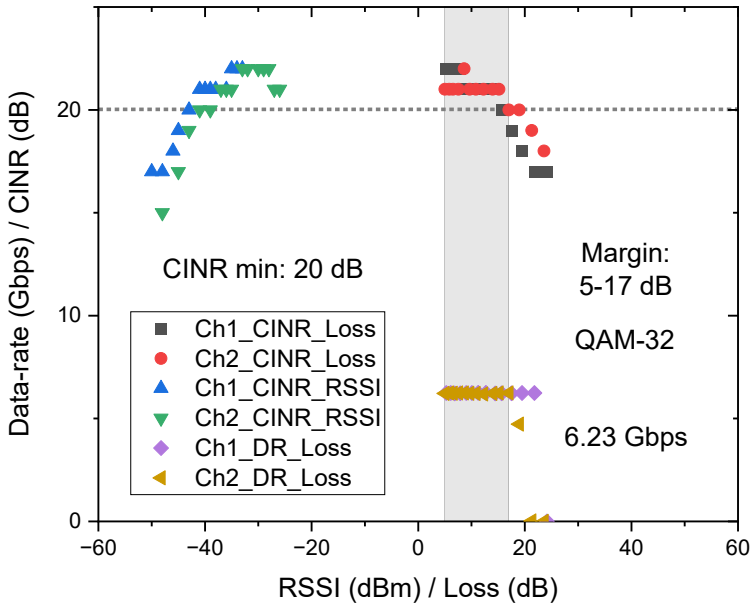

Figure 34: QAM-32 performance measurements in WR3.

The Table 7 below summarizes the QAM-32 performances and margin.

		RSSI Min	CINR Min	Data-rate (DR)	Margin
		dBm	dB	Gbps	dB
QAM-32	Ch1	-48	17	6.23	21.8
QAM-32	Ch2	-38	20	6.24	17

Table 7: Minimum performances to get a Link Up (QAM-32 modulation) in WR3.

From these measurements and in comparison with the total losses obtained previously, we can deduce the actual margin available for each modulation considering the OTA case.

		WR12 Margin	WR3 Margin	Data-rate (DR)	OTA Link budget	Penalty WR12->WR3	OTA margin
		dB	dB	Gbps	dB	dB	dB
QPSK	FDD	58.1	35	2.55	13.2	23.1	**21.8**
QAM-16	FDD	47.3	23.6	4.97	13.2	23.7	**10.4**
QAM-32	FDD	41.6	17	6.23	13.2	24.6	**3.8**
QAM-64	FDD	41.6	N/A	7.34	N/A	N/A	**N/A**
QAM-128	FDD	32.2	N/A	8.7	N/A	N/A	**N/A**

Table 8: Overview of the measured performances.

From the values in the table 8, it should be noted that the penalty observed from WR12 to WR3 is progressively degraded from QPSK to QAM-32, while in QAM-64 no link was established with good performances (e.g. data rate was lower that the DR in QAM-32). Thus the OTA PoC should work properly in QPSK and possibly in QAM16. If the THz alignment is very good.

However, in QAM32 the OTA margin is maybe too low to run the system. In relation to the PoC1, that requires fundamentally to operate around 1 Gbps for the machine to machine connections, this should not be a problem and QPSK will be targeted.

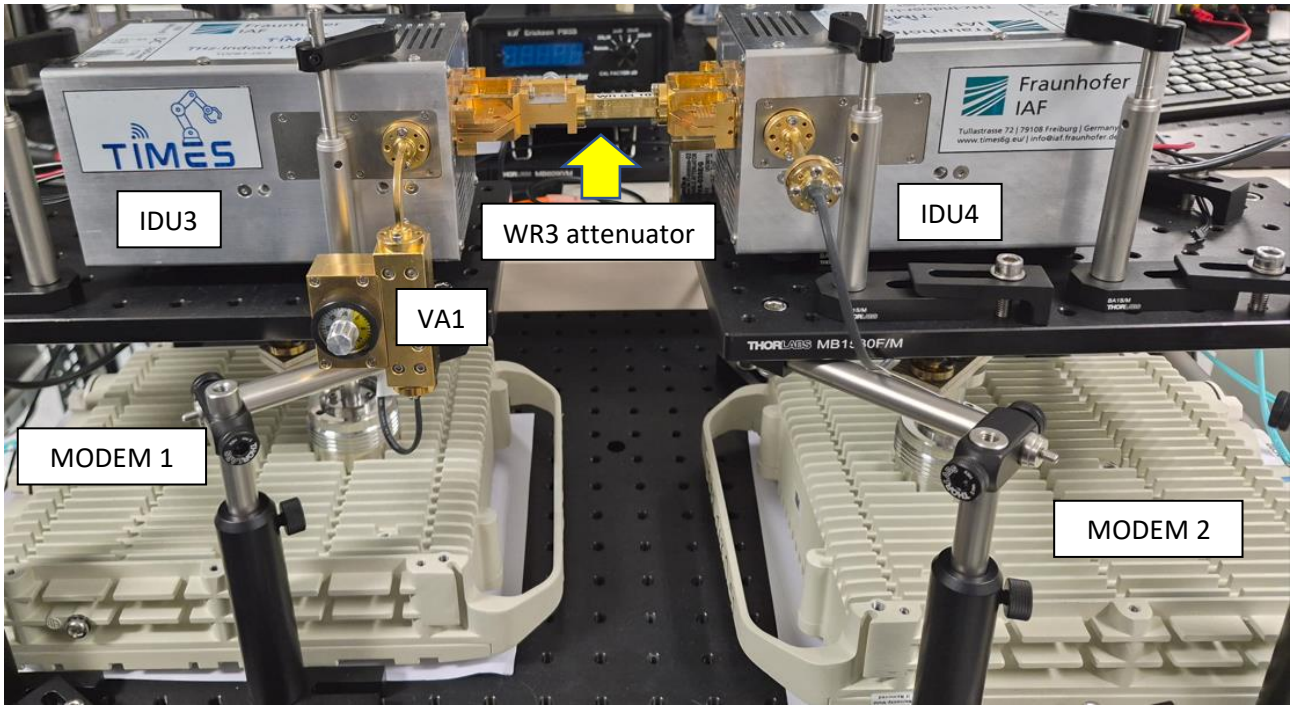

Figure 35: Photo of the PoC1 operating in Back-to-back, with a direct WR3 attenuator.

2.5 Conclusion: integration and validation of the PoC1

At this stage, the PoC1 was fully integrated and tested in the lab, with a link margin that meets the performance of the targeted scenario. The final step is to run the PoC in the over the air (OTA) case, first at CNRS and at AETNA in the last phase of the project.

3 PoC-2: Dynamic THz Link with Beam-Steering by Leaky-Wave Antenna

3.1 Introduction and Goals

In the following, Proof of Concept (PoC)-2 is described, which investigates dynamic beam steering for indoor. Terahertz (THz) wireless links using the complete end-to-end communication system. PoC-2 comprises two experimental setups that address the tracking of a Mobile Station (MS) under changing link geometry:
- frequency-controlled beam steering using a Leaky-Wave Antenna (LWA)
- beam steering using an active Reconfigurable Intelligent Surface (RIS).

In the LWA-based setup, the movement of the MS is continuously tracked by adapting the carrier frequency, exploiting the frequency-dependent radiation characteristics of the antenna. In the RIS-based setup, beam steering is realized by configuring discrete reflection states of the surface while the MS changes its position.

The following sections present laboratory-based tests conducted with the fully integrated system, including modems, THz Radio Frequency (RF) front-ends, antennas, and control interfaces. The focus is on experiments that employ the complete system under dynamic conditions representative of the PoC-2 scenario.

3.2 System Overview

This section provides an overview of the experimental setups used in PoC-2. Both setups are based on the same end-to-end THz communication system and differ only in the beam steering mechanism employed.

One setup realizes beam steering using a leaky-wave antenna at the base station, while the second setup employs an active reflective intelligent surface. In both cases, a mobile station changes its position relative to the fixed infrastructure, and the beam direction is adapted electronically without mechanical steering.

3.2.1 LWA-based setup

In the LWA-based setup, the Base Station (BS) is equipped with a leaky-wave antenna that enables frequency controlled beam steering. The BS remains at a fixed position, while the MS moves along a circular trajectory with a radius of approximately 1.5m around the BS. By adapting the carrier frequency of the transmitted signal, the main radiation direction of the LWA is steered to follow the position of the MS. The setup is designed to investigate continuous beam tracking under dynamic link geometry using a single steerable antenna element at the BS. The laboratory implementation of the LWA-based setup is shown in Figure 36.

Figure 37 illustrates the block diagram of the LWA-based PoC-2 setup and the interconnection of the individual system components at the BS and the MS. On both sides, a control unit interfaces with a Time Division Duplex (TDD) modem, which provides the bidirectional baseband and Intermediate Frequency (IF) signals required for communication. The IF signals are routed via a WR-12 splitter to the corresponding IF input and output ports of the THz indoor unit.

Within the indoor unit, frequency conversion between the IF and the RF domains is performed. The resulting RF signals are forwarded via an RF combiner to the antenna interface. At the BS, the RF combiner is connected to the LWA, which enables frequency-controlled beam steering. At the MS, the RF combiner feeds a high-gain lens-horn antenna providing a fixed and highly directive radiation pattern. Since the leaky-wave antenna

at the BS radiates with vertical polarization, a polarization rotator is inserted at the MS side to ensure polarization alignment between the transmit and receive antennas.

A wireless THz link between the BS and the MS is established. The bidirectional signal flow is supported by the same hardware chain, with transmit and receive paths sharing the RF and IF components as indicated in the block diagram. This architecture enables dynamic beam steering at the BS while maintaining a consistent end-to-end signal chain during the experiments.

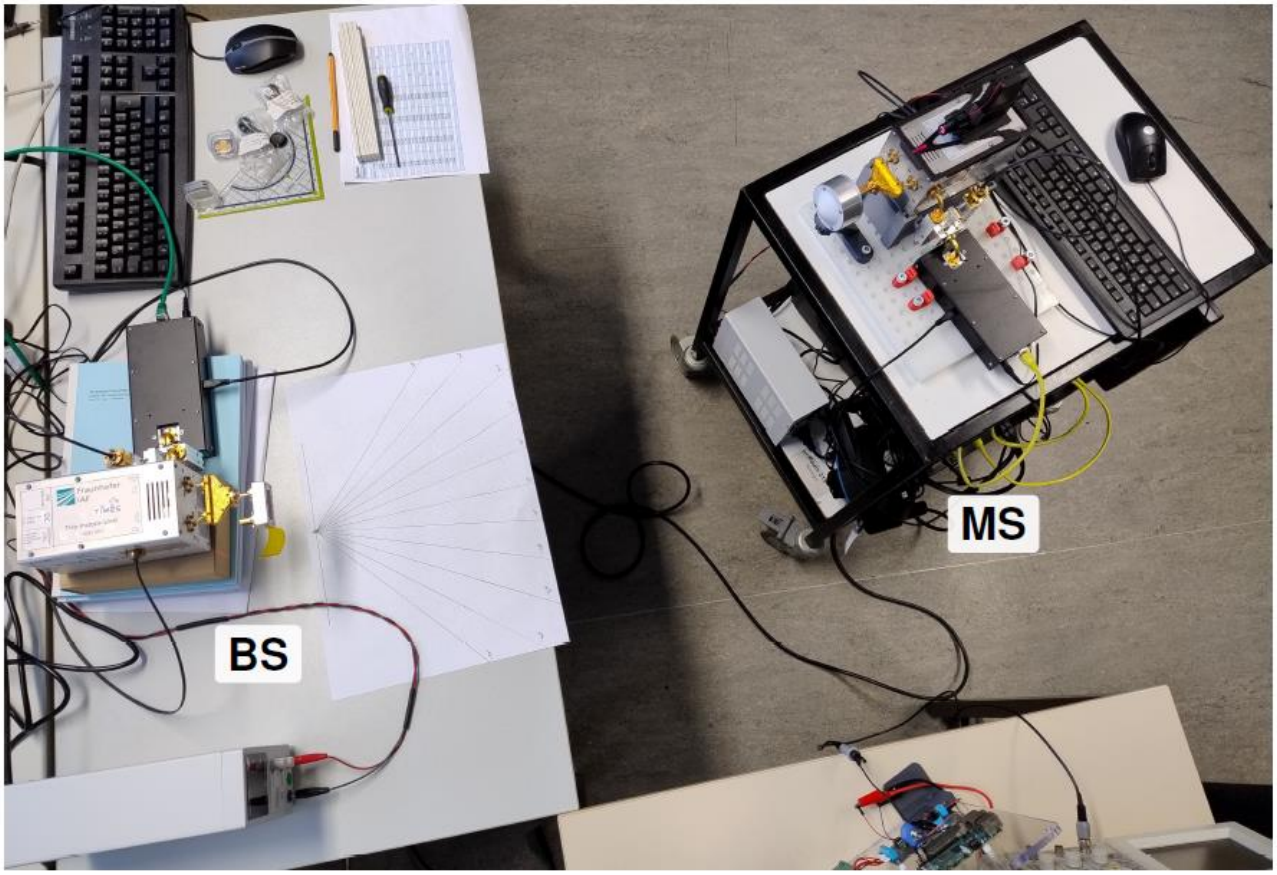

Figure 36: Laboratory setup of the LWA-based PoC-2 experiment, indicating base station (BS) and mobile station (MS).

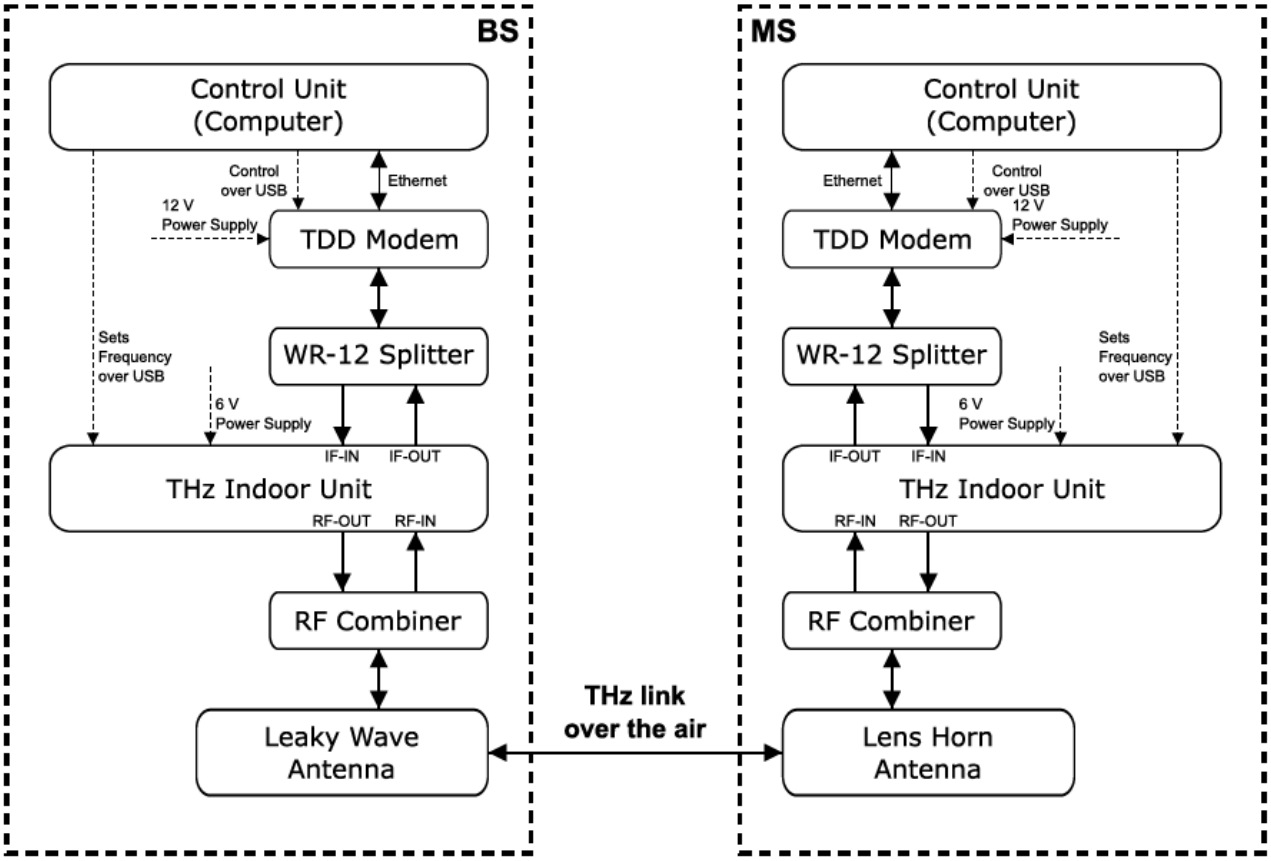

Figure 37: Block diagram of the LWA based PoC2 Setup.

3.2.2 Reconfigurable Intelligent Surface based Setup

In the RIS-based setup, beam steering is realized using an active reconfigurable intelligent surface fabricated by ANTERAL partner in TIMES, which performances are reported in the D5.4 [3]. The BS and the RIS are installed at fixed positions in the laboratory environment, while the MS moves along a circular trajectory around the RIS. Beam steering is achieved by configuring discrete reflection states of the RIS, which redirect the incident THz signal towards the MS, thereby enabling a controlled Non-Line of Sight (NLoS) propagation path.

A block diagram of the complete experimental setup is shown in Figure 38. The overall system architecture is identical to the LWA-based configuration, with the main difference being the replacement of the direct over-the air link by a RIS-assisted THz channel.

At both the BS and the MS, a control unit (computer) interfaces with a TDD modem via Ethernet. The modem output at IF is routed through a WR-12 splitter and connected to the THz indoor unit, which performs frequency up- and down-conversion to the THz band. The resulting RF signals are combined and fed to a lens horn antenna, forming a highly directive THz beam.

The wireless link between the BS and the MS is established via the active RIS, which reflects and redirects the incident THz wave towards the MS. The RIS is powered externally and configured manually using discrete

switching states that define the reflection angle during the experiment. This setup enables a controlled evaluation of RIS-assisted THz beam steering under realistic PoC conditions.

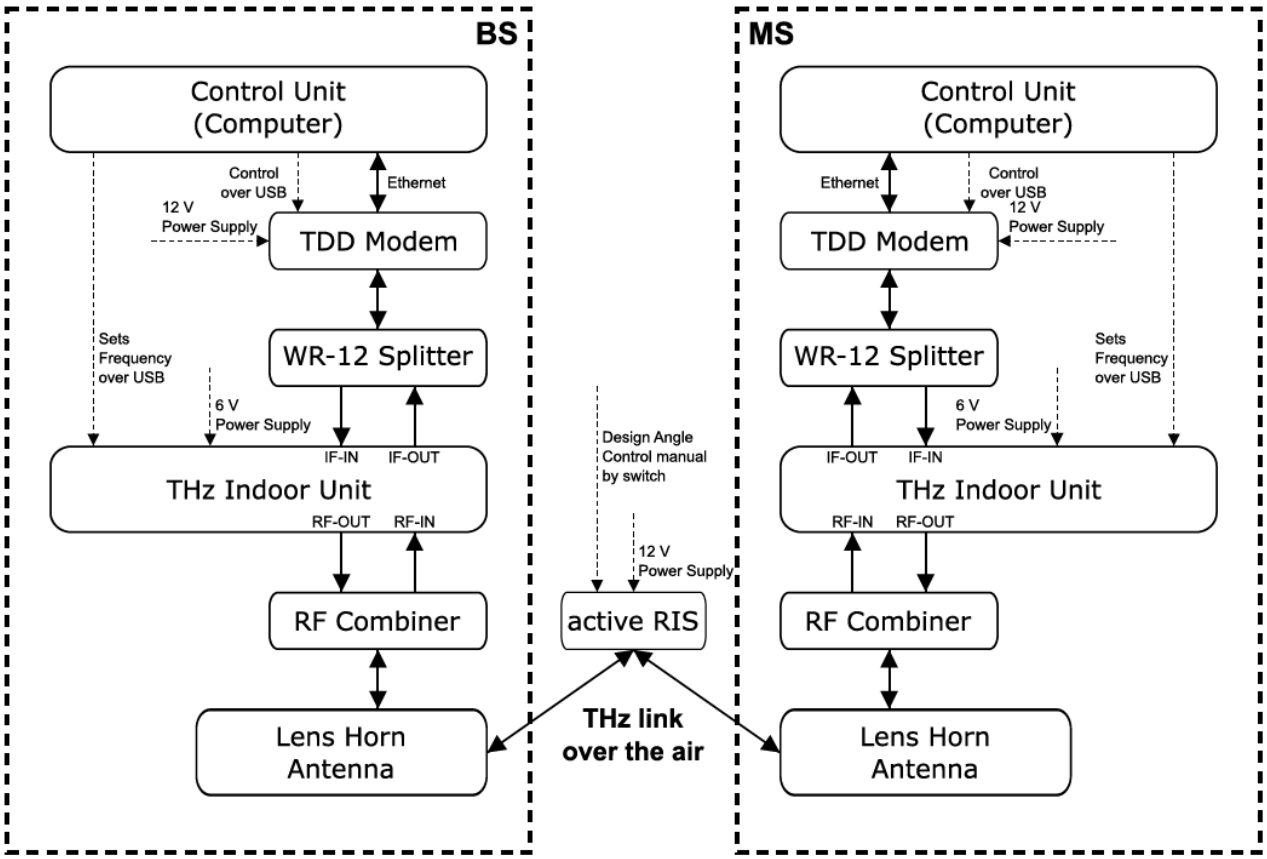

Figure 38: Block diagram of the PoC-2 THz link employing an active RIS.

3.3 Components and Equipment

In this section, the list of required equipment is detailed for the two scenarios considered for the PoC2.

Equipment used in both experimental setups

- Two computers each with connection setup
  - – USB connection from computer to THz indoor unit
  - – USB connection from computer to TDD modem
  - – 10 Gbit/s Ethernet connection to TDD modem

- Two TDD modems (HRCP), each with additional equipment
  - – 12 V power supply
  - – CAT-6 Ethernet cable

- Two TIMES indoor units, each consisting of
  - – 2 × PLL
  - – 1 × RX
  - – 1 × TX

  – 1 × HPA
  – 6 V power supply

• IF components between modems and indoor units
  – WR-12 waveguides
  – WR-12 splitter
  – WR-12 flexible waveguides

• RF components
  – WR-3.4 waveguides
  – RF combiner
  – polarisation rotator

• Mechanical mounting and positioning equipment

Equipment specific to the LWA-based setup
• Leaky-wave antenna at the BS
• High-gain lens-horn antenna at the MS

Equipment specific to the RIS-based setup
• Active reconfigurable intelligent surface with
  – RIS control interface
  – 12 V power supply
• High-gain lens-horn antenna at the BS and the MS

3.4 LWA and RIS performances

3.4.1 Leaky Wave Antenna

This section summarizes the main results concerning the LWA. Readers wishing to learn more are invited to refer to deliverable D5.3 [2].

The two important metrics for this antenna are gain and steering capability.

For the steering performance, Figure 39 shows the normalized gain in the $\varphi = 0°$ direction measured as a function of frequency. The evolution of the maximum normalized gain, which steered, with frequency is clearly visible.

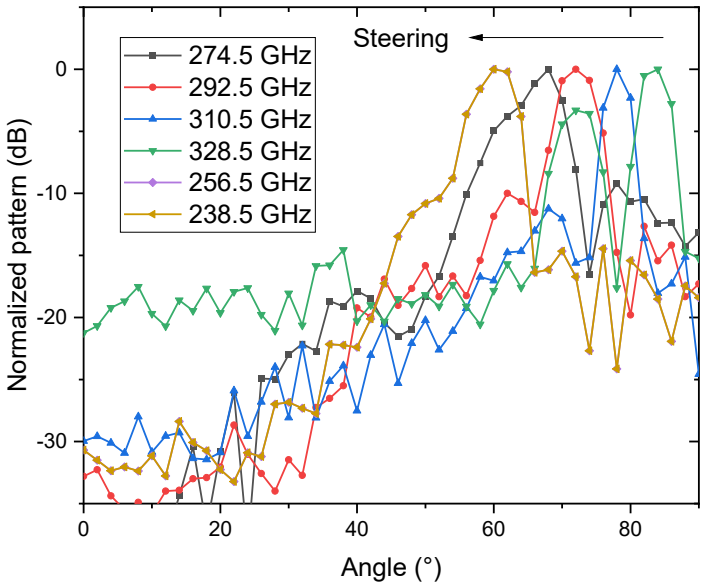

Figure 39: Steering performance of LWA.

To be more quantitative, Figure 40 presents the LWA's steering performance. Even though a 7-8% difference is observed between simulations and measurements, the frequency steering is clearly visible with a rate of approximately 0.34°/GHz.

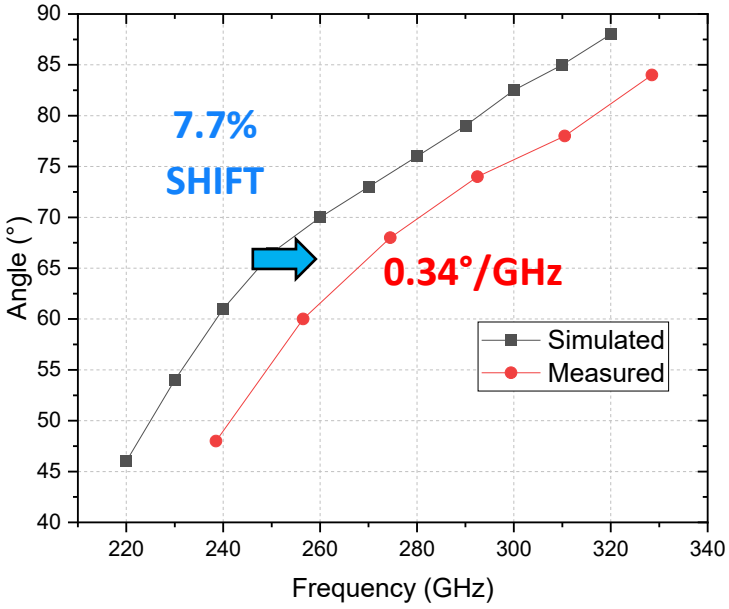

Figure 40: Comparison between simulations and measurements about the steering performance.

Finally, the actual gain of the LWA can be obtained and compared with the simulations as shown in Figure 41. Even though a difference of 13 dB is observed between simulations and measurements, the LWA still exhibits a gain greater than 10 dB over a bandwidth of approximately 50 GHz.

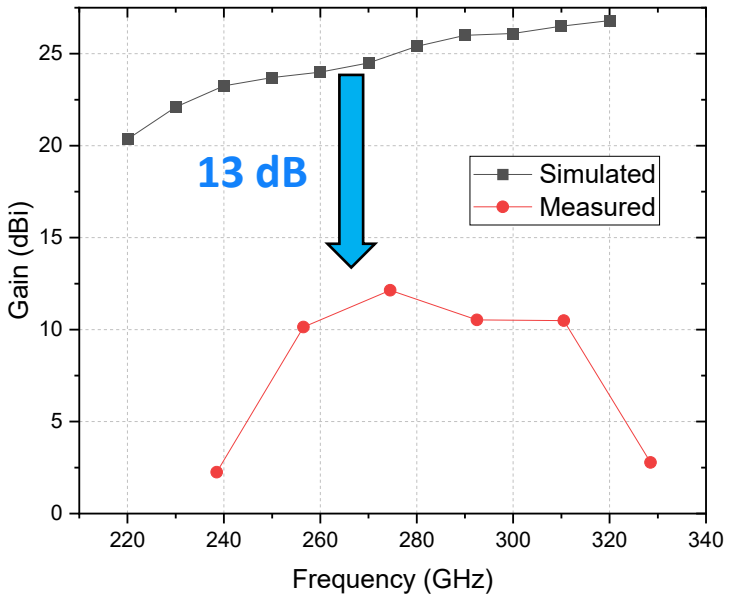

Figure 41: Actual gain of the LWA in comparison with the simulations.

3.4.2 Reflective Intelligent Surface

This section summarizes the main results concerning the characterization of the liquid crystal based reconfigurable RIS. Readers wishing to learn more are invited to consult deliverable D5.4 [3].

Figure 42 shows a horizontally oriented image of the reconfigurable RIS:

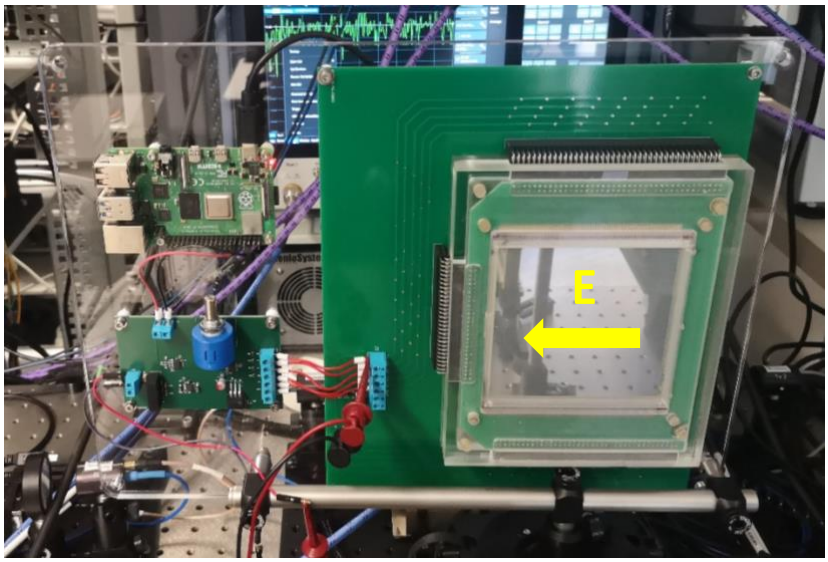

Figure 42: Photograph of the reconfigurable RIS with the incoming polarization.

It is also important to point out that polarization is important when using this IRS. Specifically, the yellow arrow in the Figure 42 represents the E-field for incoming THz beam.

Thus, if the field is not oriented in this way, we obtain a specular response as shown in Figure 43.

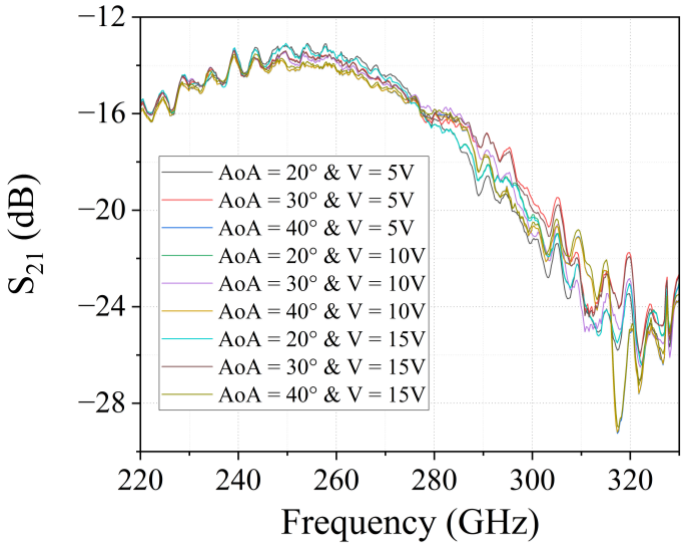

Figure 43: Specular response of the substrate in terms of AoA and voltage.

The maximum amplitude for the S_{21} is approximately -16 dB at 280 GHz. This is the value used for comparison with measurements in a non-specular configuration.

If we now align the field correctly, still in a specular configuration, we obtain the Figures 44.a and 44.b, which show the evolution of absorption as a function of the applied voltage for 2 values of AoA.

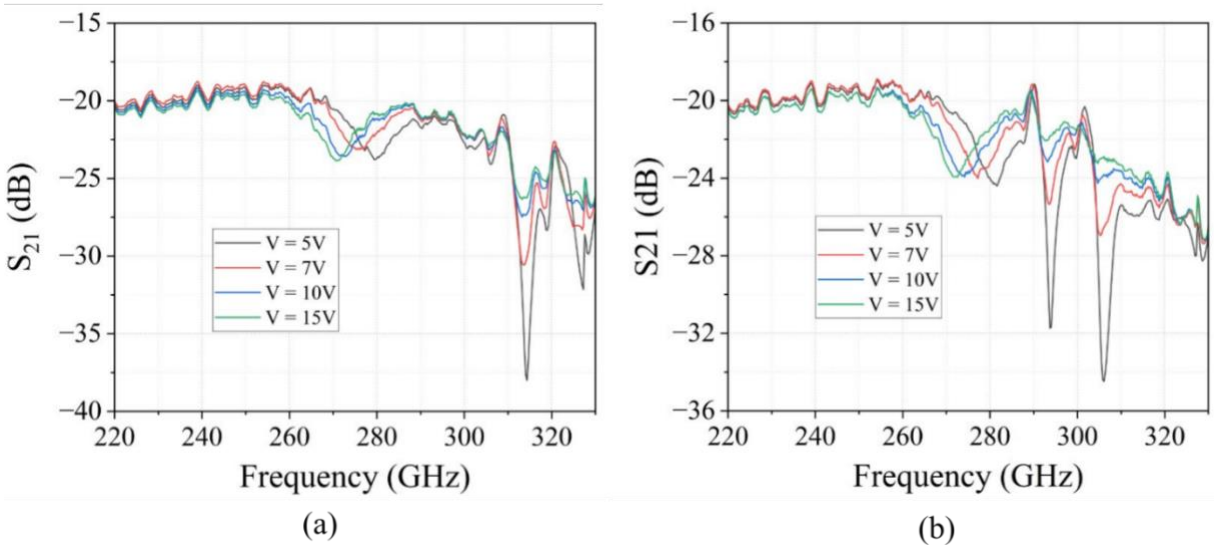

Figure 44: Specular response of the reconfigurable RIS for different voltages and for (a) AoA = AoD = 20° and (b) AoA = AoD = 30°.

The absorption band is approximately 25 GHz (between 260 and 285 GHz) with an amplitude of approximately 4.5 dB. There is also a clear impact of the applied voltage, which has the effect of “redshifting” the absorption peak.

Finally, we present the results obtained in the non-specular configuration (where IRS effect is expected) for two different AoAs AoA = 0° (Figure 45) and AoA = 40° (Figure 46).

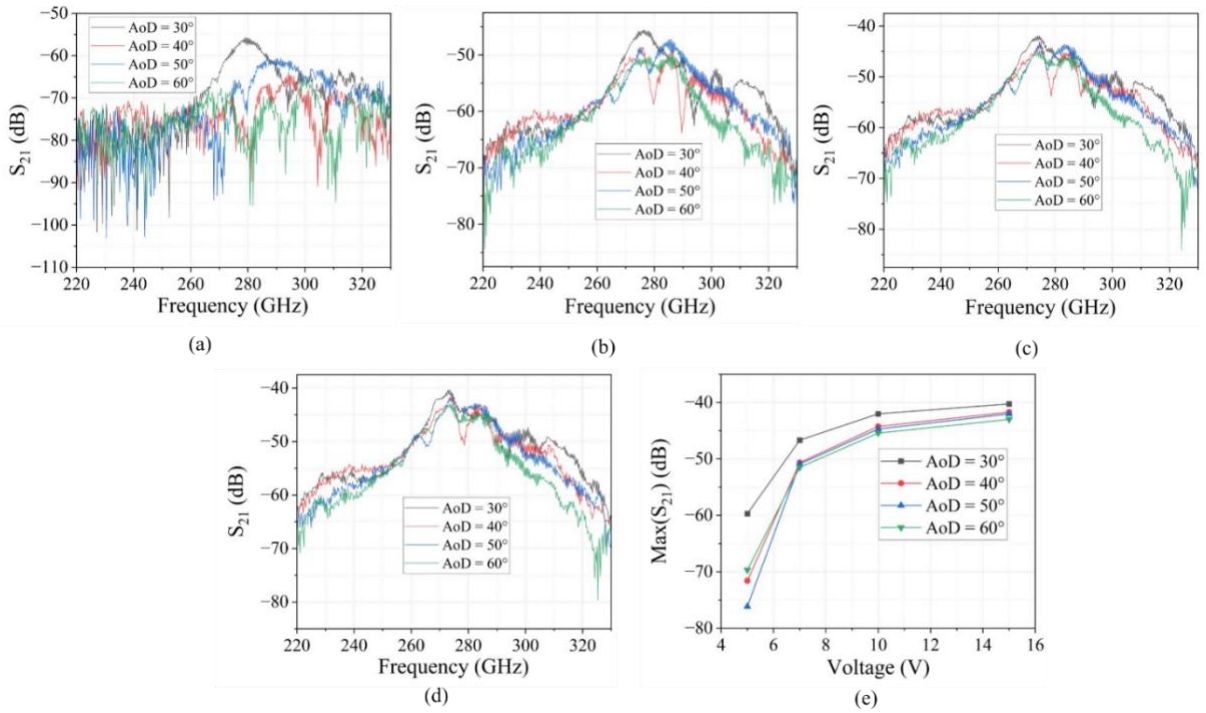

Figure 45: Amplitude of S21 in the nonspecular case for AoA = 0° for an applied voltage of (a) 5V, (b) 7V, (c) 10V and (d) 15V. (e) Maximum of S21 at optimal frequency f = 273.35 GHz.

For AoA = 0°, an emission peak is visible for each applied voltage value, although beyond 10 Vpp, the change is not significant. This is certainly a sign that the saturation voltage for the liquid crystals has been reached. It is important to note that at 15 Vpp, the maximum of the S21 is approximately -40 dB at 273.35 GHz for the configuration (AoA = 0°, AoD = 30°), therefore about 24 dB different from the measurement in the specular configuration.

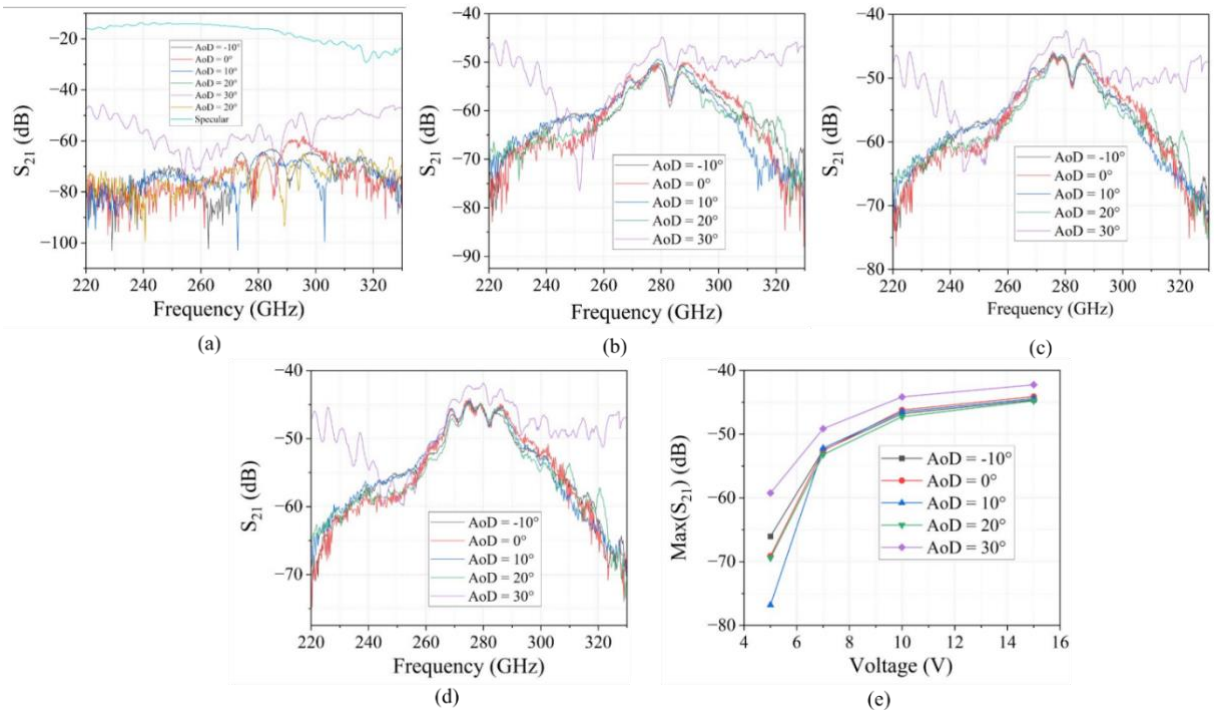

Figure 46: Amplitude of S21 in the nonspecular case for AoA = 40° for an applied voltage of (a) 5V, (b) 7V, (c) 10V and (d) 15V. (e) Maximum of S21 at optimal frequency f = 275 GHz.

For an AoA = 40°, the results are similar but only reach a maximum S21 of -45 dB at a frequency of 275 GHz for an AoD = 0° so about 30 dB loss compared to substrate in specular configuration.

3.5 Experimental results

Table 10 summarizes the measured link performance for Channel 2 as a function of the applied LO and resulting RF frequency. Channel 2 was selected for the evaluation, as it consistently provided better performance compared to the other available channel. For several frequency settings, according the the LWA expected gain, we confirmed that no stable link could be established, which is indicated by missing values in the table.

However, for the frequency range between approximately 272GHz and 297 GHz, stable wireless links were achieved with maximum communication distances between 1m and 1.6 m. The maximum supported data rates vary significantly across the investigated frequencies, ranging from a few hundred Mbit/s up to 1800 Mbit/s, validating the use of the LWA in the THz channel.

The highest data rates were observed at several discrete RF frequencies, while at other frequencies the achievable data rate was limited despite similar link distances.

Overall, the results demonstrate a strong dependence of both achievable distance and data rate on the selected RF frequency. This behavior reflects the frequency-dependent radiation characteristics of the leaky-wave antenna as well as the sensitivity of the end-to-end link budget to the operating frequency in the considered THz band.

LO Frequency (GHz)	RF Frequency (GHz)	Max. Distance (m)	Max. Data Rate (Mbit/s)
26.0	268.48	-	-
26.4	271.68	1	900
26.8	274.88	1	420
27.2	278.08	1.4	1800
27.6	281.28	1.6	800
28.0	284.48	1.5	400
28.4	287.68	1.5	1300
28.8	290.88	1	1500
29.2	294.08	1.1	1400
29.6	297.28	1.1	240
30.0	300.48	-	-
30.4	303.68	-	-
31.2	310.08	1	1800
32.0	316.48	1.1	300
32.8	322.88	-	-

Table 10: Measured link performance for Channel 2 as a function of LO and RF frequency.

4 Conclusions

In this document, we reported on the two PoCs that are on-going in the TIMES projet. Main conclusions are shortly summarized hereafter.

- The PoC1 uses the fixed RIS and a FDD approach. The PoC1 has been fully integrated and validated in waveguide and the obtained link budget is in line with the expectations of the industrial PoC targeted in AETNA. The performances have been detailed and they are fully compliant with the targeted demo. This demo will happen at AETNA, ahead of the final meeting in march.

- The PoC2 that targets a TDD link in the 300 GHz has been validated up to 1.6 m using the leak-wave antenna and a mobile receiver. The performances of the link in terms of data-rates were fixed by the MODEM itself and available link budget, including the IDUs and the antenna gains.

- The last phase of the PoC2 is the use of the reconfigurable RIS and is so far on-going at TUBS.

5 References

[1] TIMES deliverable (D2.3) "Definition of the scenarios and KPI for hardware demonstration and PoC", Available on TIMES Website, http://www.times6g.eu/deliverables.

[2] TIMES deliverable (D5.3) "Design, fabrication and verification of high directivity and beam steering antennas at THz frequencies", Available on TIMES Website, http://www.times6g.eu/deliverables.

[3] Times deliverable (D5.4) "Development and validation of IRS-based THz links", Available on TIMES Website, http://www.times6g.eu/deliverables.

[4] Times deliverable (D6.2) "Integration and validation of MODEM+RF Front ends", Available on TIMES Website, http://www.times6g.eu/deliverables.